NBS TECHNICAL NOTE 871

U.S. DEPARTMENT OF COMMERCE / National Bureau of Standards

Geometrical Calibration of the NBS Electron Scattering Apparatus

NATIONAL BUREAU OF STANDARDS

The National Bureau of Standards[1] was established by an act of Congress March 3, 1901. The Bureau's overall goal is to strengthen and advance the Nation's science and technology and facilitate their effective application for public benefit. To this end, the Bureau conducts research and provides: (1) a basis for the Nation's physical measurement system, (2) scientific and technological services for industry and government, (3) a technical basis for equity in trade, and (4) technical services to promote public safety. The Bureau consists of the Institute for Basic Standards, the Institute for Materials Research, the Institute for Applied Technology, the Institute for Computer Sciences and Technology, and the Office for Information Programs.

THE INSTITUTE FOR BASIC STANDARDS provides the central basis within the United States of a complete and consistent system of physical measurement; coordinates that system with measurement systems of other nations; and furnishes essential services leading to accurate and uniform physical measurements throughout the Nation's scientific community, industry, and commerce. The Institute consists of a Center for Radiation Research, an Office of Measurement Services and the following divisions:

Applied Mathematics — Electricity — Mechanics — Heat — Optical Physics — Nuclear Sciences[2] — Applied Radiation[2] — Quantum Electronics[3] — Electromagnetics[3] — Time and Frequency[3] — Laboratory Astrophysics[3] — Cryogenics[3].

THE INSTITUTE FOR MATERIALS RESEARCH conducts materials research leading to improved methods of measurement, standards, and data on the properties of well-characterized materials needed by industry, commerce, educational institutions, and Government; provides advisory and research services to other Government agencies; and develops, produces, and distributes standard reference materials. The Institute consists of the Office of Standard Reference Materials and the following divisions:

Analytical Chemistry — Polymers — Metallurgy — Inorganic Materials — Reactor Radiation — Physical Chemistry.

THE INSTITUTE FOR APPLIED TECHNOLOGY provides technical services to promote the use of available technology and to facilitate technological innovation in industry and Government; cooperates with public and private organizations leading to the development of technological standards (including mandatory safety standards), codes and methods of test; and provides technical advice and services to Government agencies upon request. The Institute consists of a Center for Building Technology and the following divisions and offices:

Engineering and Product Standards — Weights and Measures — Invention and Innovation — Product Evaluation Technology — Electronic Technology — Technical Analysis — Measurement Engineering — Structures, Materials, and Life Safety[4] — Building Environment[4] — Technical Evaluation and Application[4] — Fire Technology.

THE INSTITUTE FOR COMPUTER SCIENCES AND TECHNOLOGY conducts research and provides technical services designed to aid Government agencies in improving cost effectiveness in the conduct of their programs through the selection, acquisition, and effective utilization of automatic data processing equipment; and serves as the principal focus within the executive branch for the development of Federal standards for automatic data processing equipment, techniques, and computer languages. The Institute consists of the following divisions:

Computer Services — Systems and Software — Computer Systems Engineering — Information Technology.

THE OFFICE FOR INFORMATION PROGRAMS promotes optimum dissemination and accessibility of scientific information generated within NBS and other agencies of the Federal Government; promotes the development of the National Standard Reference Data System and a system of information analysis centers dealing with the broader aspects of the National Measurement System; provides appropriate services to ensure that the NBS staff has optimum accessibility to the scientific information of the world. The Office consists of the following organizational units:

Office of Standard Reference Data — Office of Information Activities — Office of Technical Publications — Library — Office of International Relations.

---

[1] Headquarters and Laboratories at Gaithersburg, Maryland, unless otherwise noted; mailing address Washington, D.C. 20234.
[2] Part of the Center for Radiation Research.
[3] Located at Boulder, Colorado 80302.
[4] Part of the Center for Building Technology.

Geometrical Calibration of the NBS Electron Scattering Apparatus

S. Penner, S. P. Fivozinsky,
and J. W. Lightbody, Jr.

Nuclear Sciences Division
Institute for Basic Standards
National Bureau of Standards
Washington, D.C. 20234

L. S. Cardman

University of Illinois
Champaign, Illinois 61801

W. P Trower

Virginia Polytechnic Institute and
State University
Blacksburg, Virginia 24061

Sponsored by

Research Corporation of New York
405 Lexington Avenue
New York, New York 10017

and

U.S. Energy Research and Development Administration
Washington, D.C. 20545

U.S. DEPARTMENT OF COMMERCE, Rogers C.B. Morton, *Secretary*
NATIONAL BUREAU OF STANDARDS, Richard W. Roberts, *Director*

Issued June 1975

National Bureau of Standards Technical Note 871

Nat. Bur. Stand. (U.S.), Tech. Note 871, 79 pages (June 1975)

CODEN: NBTNAE

U.S. GOVERNMENT PRINTING OFFICE
WASHINGTON: 1975

For sale by the Superintendent of Documents, U.S. Government Printing Office, Washington, D.C. 20402
(Order by SD Catalog No. C13.46:871). Price $1.40 (Add 25 percent additional for other than U.S. mailing.)

CONTENTS

ILLUSTRATIONS

Geometrical Calibration of the NBS Electron Scattering Apparatus

S. Penner, S. P. Fivozinsky, J. W. Lightbody, Jr.,
L. S. Cardman, and W. P. Trower

A comprehensive calibration of the geometry of the NBS electron scattering apparatus is described. A complete set of measured parameters is tabulated in this report. Combining these parameters with observed values of certain variables as described herein permits the accurate determination of the solid angle, scattering angle, and target angle for each cross section measurement made with the apparatus. The uncertainty in a cross section measurement due to the imprecision of the geometry calibrations is less than one part in 10^3.

Key Words: Absolute cross section; beam profile; electron scattering; scattering angle; solid angle; spectrometer.

I. Introduction

The ability to determine absolute elastic electron scattering cross sections to very high accuracy is being developed by the NBS electron scattering group for several reasons:

to establish the charge distribution of the proton, a fundamental object,

to establish precise cross sections for carbon which are widely used as a standard in relative measurements of other electron scattering cross sections, both elastic and inelastic, and

to determine the importance of dispersive effects in electron scattering.

To make significant contributions to the solution of these problems, an overall cross section measurement accuracy well below one percent must be achieved. A careful examination of all the factors influencing the overall accuracy of cross section measurements has been made, and we have concluded that the desired accuracy is obtainable [1].[1] Among the many experimental factors which must be understood are those related to the geometry of the apparatus.

In the following sections of this report, we describe those parts of the NBS electron scattering apparatus [2] which determine the geometry, define the coordinate systems used and the quantities to be measured, describe the measurements which are made, and discuss

[1] Figures in brackets indicate the literature references on page 66.

the sources of error which affect the accuracy of measured cross sections.

II. Description of Apparatus

The NBS electron scattering apparatus is shown in figure 1. The detector system and shielding platform which are mounted to the upper half of the spectrometer magnet are omitted from this figure for clarity.

The energy-resolved electron beam is incident from the right in figure 1, in a 4-inch diameter vacuum pipe. The beam is approximately one-half inch in diameter when it enters the magnetic field of the quadrupoles. The beam is focused by the quadrupoles to a spot of less than 1 mm diameter at the target. After leaving the quadrupoles, the beam passes through the upstream beam profile scanners, whose function is to measure the size and position of the beam at this point. The beam then passes through a non-intercepting current monitor which is part of the charge measuring system [3]. The beam pipe diameter is reduced to two inches between the current monitor and the scattering chamber. In order to be able to determine the beam direction at the target, the region between the upstream beam scanners and the target is kept free of magnetic fields by wrapping the pipe with magnetic shielding. The scattering chamber is an 18-inch diameter vertical aluminum cylinder. Ports on the scattering chamber at 17.5° intervals between 40 and 162.5° allow direct connection of the beam-line and the spectrometer vacuum systems. The scattering chamber which is mounted on the target support assembly contains the target-location beam profile scanners. Downstream of the target chamber, the beam passes through a short section of 4-inch vacuum pipe followed by a long section of 12-inch pipe before entering the Faraday Cup. Scattered electrons pass through one of the scattering chamber ports into the spectrometer. The aperture slits, which are rigidly attached to the spectrometer magnet, define the scattering angle and the acceptance solid angle of the spectrometer. The high-resolution spectrometer magnet is mounted on a carriage which permits radial motion of the magnet. This carriage is mounted on the rotating base which permits changing the scattering angle. The spectrometer, aperture slits, target support assembly, and upstream beam scanners define the system geometry. We now describe these components in detail.

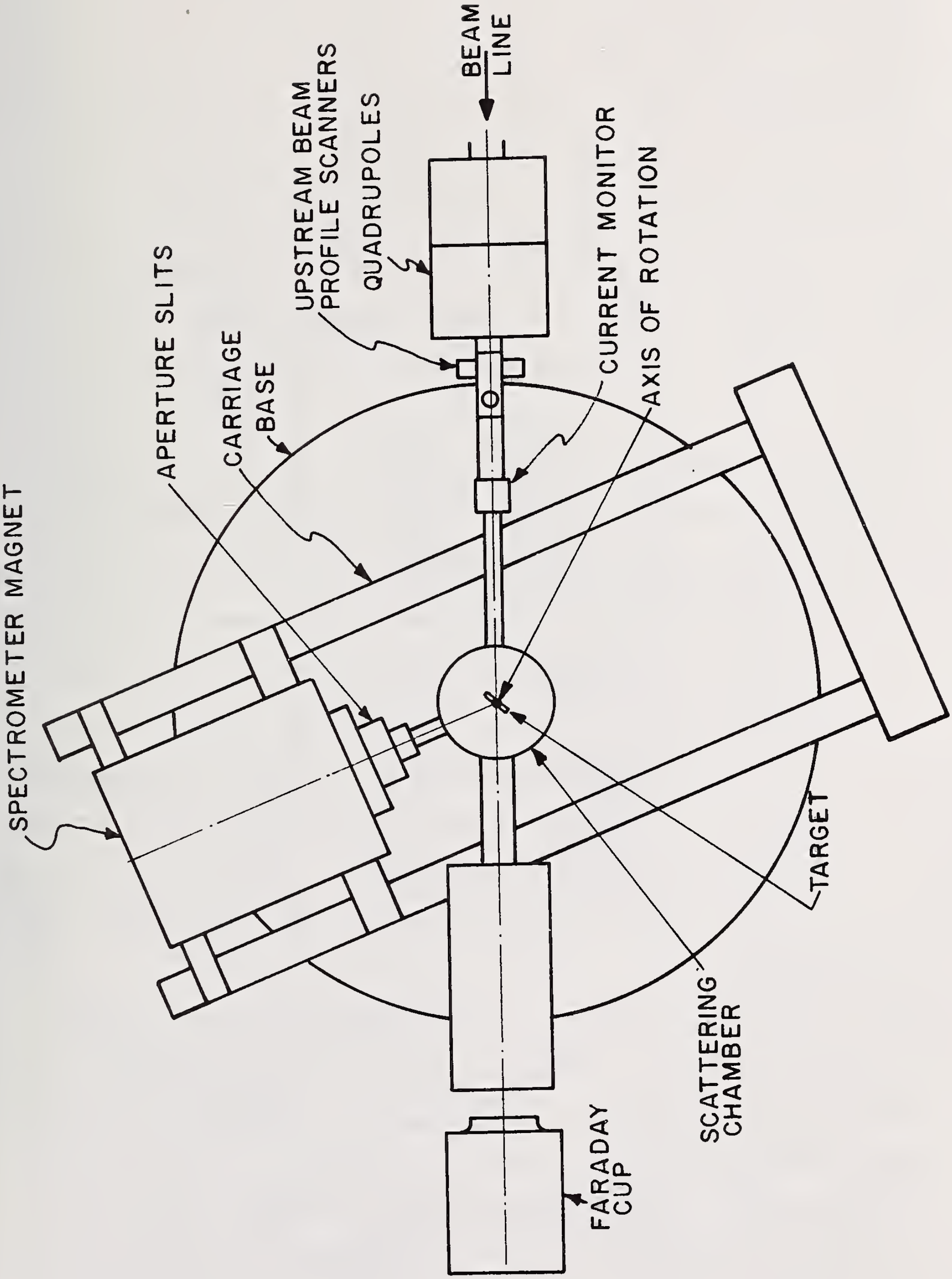

Figure 1. Plan view of electron scattering apparatus.

A. Spectrometer

The spectrometer magnet [4], shown in figure 2, has a bending radius of 76 cm, a deflection angle of 169.8°, and a resolution capability of 2×10^{-4}. The detection system for scattered electrons is rigidly attached to the spectrometer exit flange [5]. Since the spectrometer acceptance angles are completely determined by the aperture slits, the magnet has no direct effect on the experimental geometry. Because the aperture slit box is rigidly attached to the magnet, motion of the magnet does affect the geometry. The magnet, which is fixed to its carriage by two main support bolts and the shielding supports, is not completely rigid. The effect of this lack of rigidity on the reproducibility of scattering angle and solid angle calibrations is small, and has been taken into account in the error analysis.

Radial motion of the spectrometer is needed in order to connect the spectrometer vacuum system to the appropriate port of the scattering chamber. The two main beams of the carriage ride on the carriage support beams through several sets of roller bearings. The support beams are an integral part of the rotating base. A hand-operated drive screw which connects the carriage and the rotating base provides radial motion. The radial position of the spectrometer is measured by means of a dial gauge mounted on the rotating base with its plunger engaging one of the cross members of the carriage. Like all the dial gauges used in the apparatus, the radial dial gauge has a nominal travel of one inch, a least count of 0.001 inch, and a standard deviation of about 0.0002 inches.[2] The gauge is located about two feet below and to the side of the center of the aperture, with its plunger aligned in the direction of carriage motion.

In addition to the roller bearings which support the carriage, there are roller bearings which engage the sides of the support beams to prevent sideways motion of the carriage on its support. This arrangement is not completely satisfactory. Small, non-reproducible motions of the spectrometer on the base are found to accompany radial displacement of the carriage. In addition, there is a small transverse component of the spectrometer motion coupled to the radial motion. Measurements of the transverse position of the aperture slit box as a function of radial spectrometer position are shown in figure 3.

---

[2] Most of the dimensions given in this report will be quoted in customary units, since the instruments used for the calibrations all read out directly in inches.

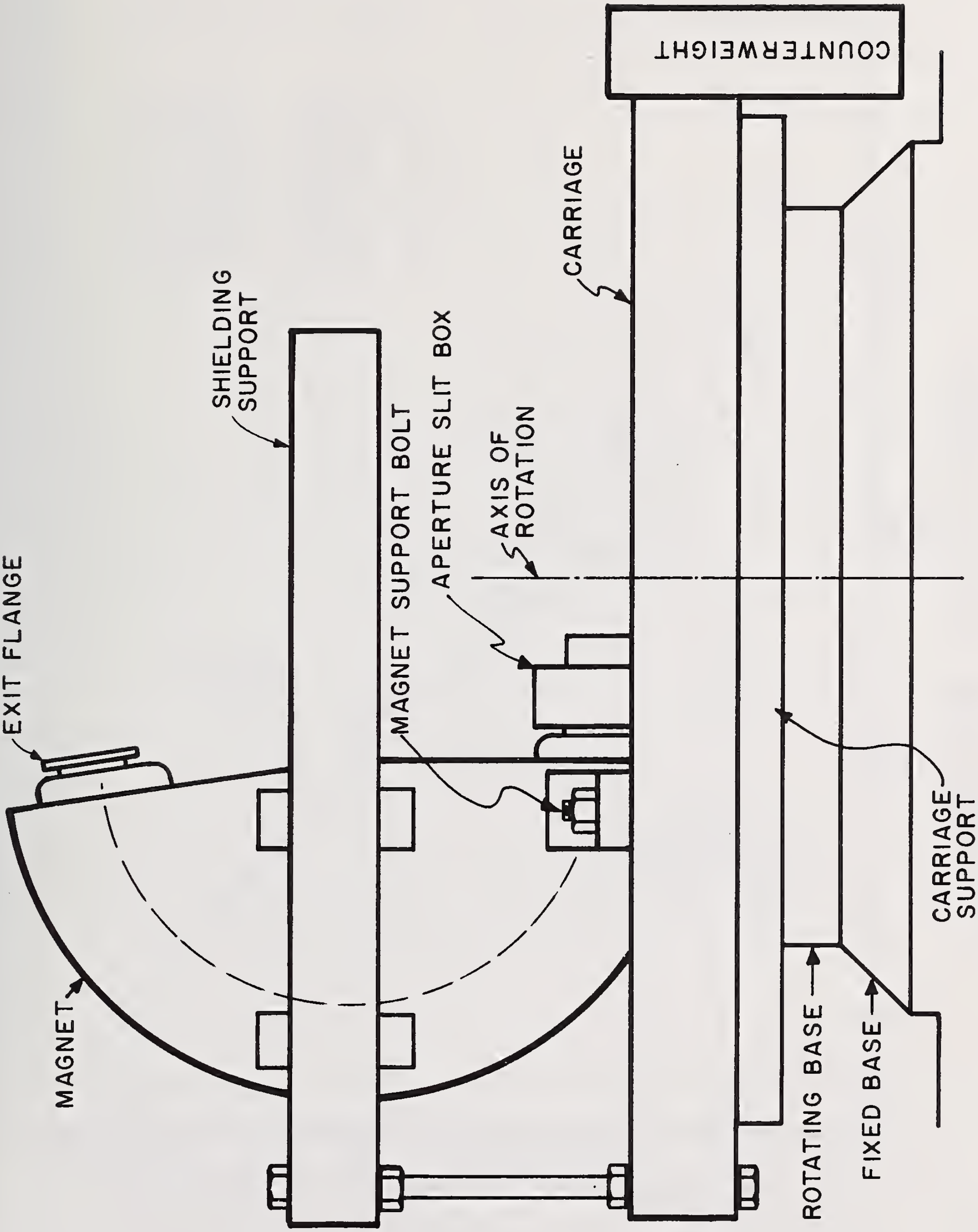

Figure 2. Electron scattering spectrometer side view.

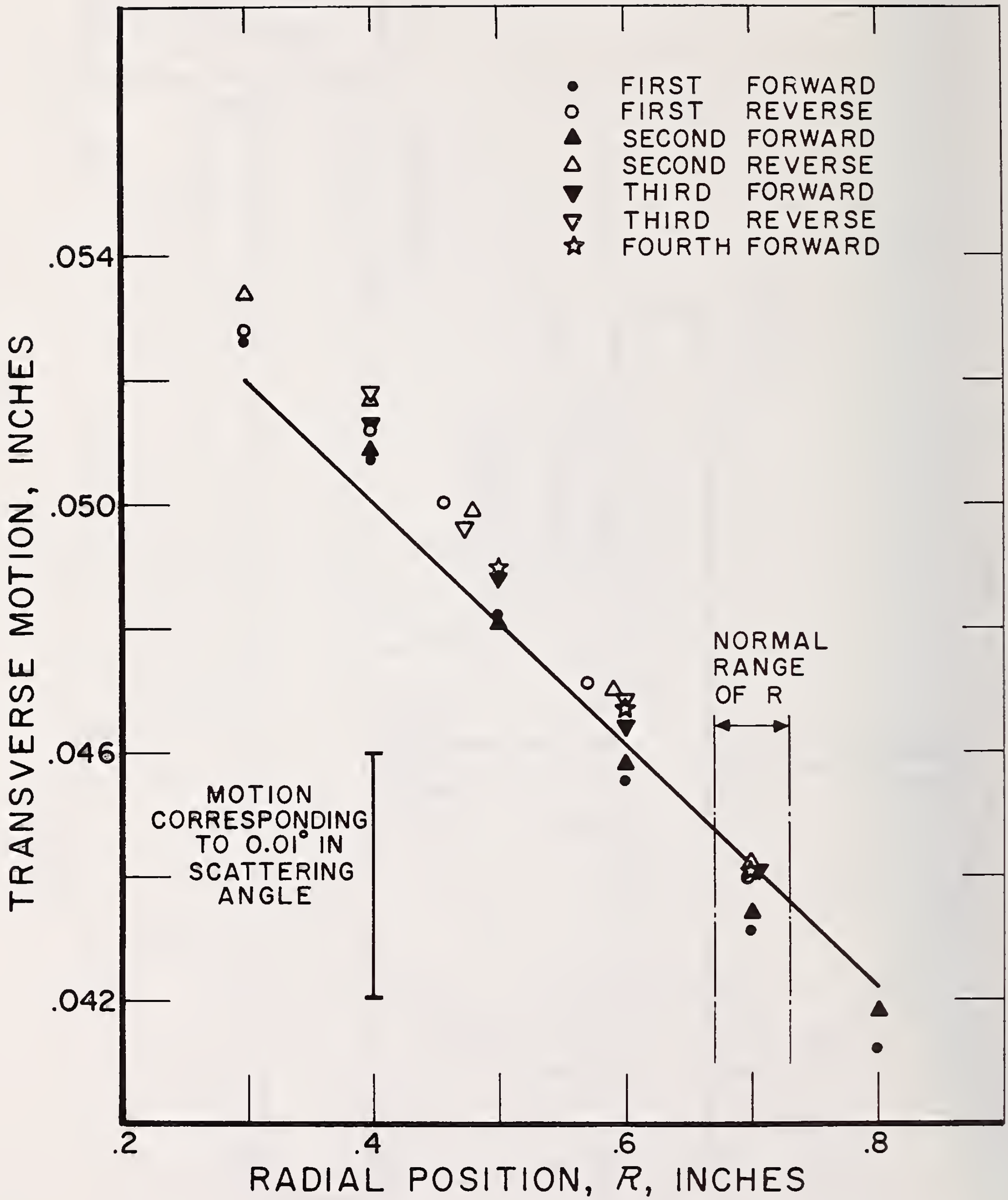

Figure 3. Transverse motion of spectrometer aperture accompanying radial motion. The solid curve indicates the motion predicted from the change of scattering angle with radial position.

The variations in transverse position at a given radial position are of order 0.001 inches, corresponding to a variation in scattering angle of 0.002 degrees. The systematic change in transverse position agrees with independent observations of the variation of scattering angle with radial position. The latter measurements will be discussed later. Because of these effects, a radial dial gauge reading is needed for each setting of the scattering angle in order to determine the exact scattering angle.

The rotating base of the spectrometer rides on the fixed base by means of a tapered roller bearing approximately six feet in diameter. A motor-driven ring and pinion gear arrangement rotates the spectrometer to change the scattering angle. Small rotations can be made manually by turning one of the gears in the speed reduction drive from the motor. The fixed portion of the spectrometer base rests on a concrete pedestal and is attached by a number of large bolts. During installation, the base was carefully leveled on steel wedges and then grouted in place. The concrete pedestal which rests directly on the four-foot thick reinforced concrete subflooring provides rigidity for the entire structure.

The spectrometer does not execute a pure rotation about a fixed axis because of imperfections in the main bearing, carriage support, and mounting of the spectrometer to the carriage. The geometry of the apparatus can nonetheless be completely determined using fixed reference points, arbitrarily defined, which are reproducible and accessible to measurement. The structural imperfections do cause motions of the apparatus which are not completely reproducible. Thus, a major part of the geometry calibration is the determination of the size of these "random" effects. The random motions are found to be small enough so that the geometrical calibrations are meaningful at the desired level of accuracy.

B. Aperture Slits

A sophisticated aperture slit system has been developed to obtain the desired solid angle accuracy. The spatial extent of the electron beam at the target, penetration of slit edges by the scattered electrons, and the desire to have a variable aperture in order to optimize count rates were important factors in the design of the aperture system. Figure 4 is a photograph of the slit box showing the four tungsten cylinders which define the aperture.

The circular cross section of the defining elements minimizes slit edge penetration

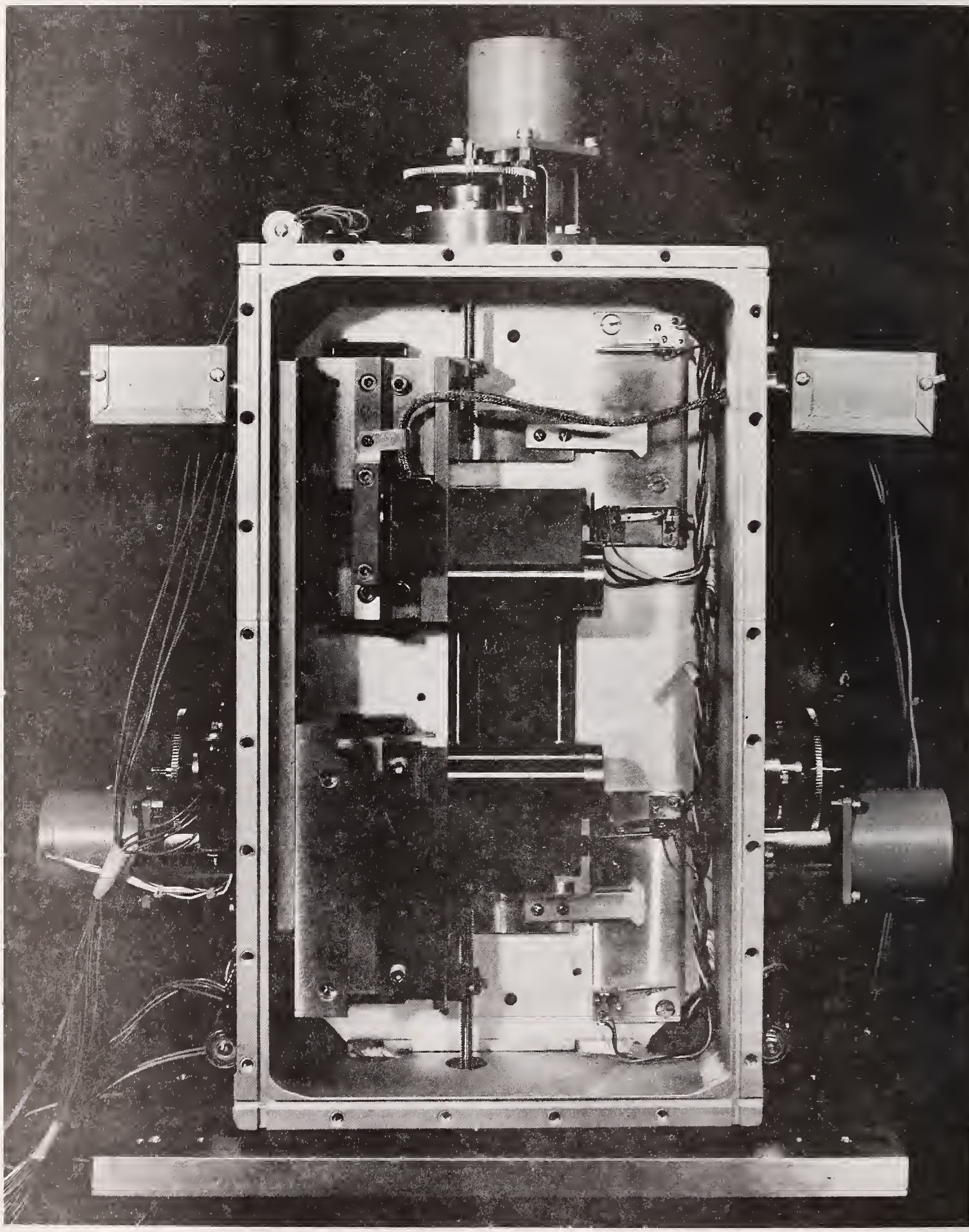

Figure 4. Photograph of Aperture Slit Assembly.

and makes the penetration depth independent of the direction of arrival of the electrons. In figure 5, line A-A represents an electron which is tangent to the slit edge. Line B-B represents an electron which penetrates the slit by a perpendicular distance ε, passing through a thickness $t(\varepsilon)$ of tungsten. For small values of ε, the circular cross section results in larger values of t than any sharp-edged slit geometry. Furthermore, the value of ε needed to obtain a given value of t is independent of the direction of electron travel (in the plane, at least), which would certainly not be the case in any slit geometry with plane surfaces.

Since the resolution of our spectrometer is better than 100 keV for electron energies up to 120 MeV, it is safe to assume that an electron which loses more than one MeV by ionization in the slit edges will not be counted in the elastic scattering peak. In tungsten, this requires $t(\varepsilon) = 0.086$ cm. The cylinders have a radius $R_s = 0.875$ inches, so that $\varepsilon = 10^{-3}$ mm for one MeV energy loss. Multiple scattering will further reduce the effective value of ε, and therefore slit edge penetration is always negligible relative to other uncertainties in establishing the true solid angle.

The vertical acceptance angle of the spectrometer is defined by a pair of cylinders whose axes are horizontal and parallel to each other. The plane defined by these axes is perpendicular to the spectrometer optic axis. The cylinders are moved independently on precise ball-bushing guides by stepping motors, in a direction perpendicular to their axes and in their original plane.

The horizontal acceptance angle is defined by the second pair of cylinders, whose axes are vertical and motion horizontal. The plane defined by the axes of this pair is accurately parallel to the plane defined by the first pair.

The construction accuracy of the slits has been carefully checked using gauge blocks and a reference right circular cylinder. Because the tungsten slits are very heavy, all measurements were made with the slit box in the same orientation as that in which it is used. Each cylinder of a pair remains parallel to the other within 10^{-4} radians throughout their entire range of motion. The two pairs of cylinders are orthogonal to each other to similar angular accuracy, and the planes defined by the two pairs are also parallel to similar accuracy.

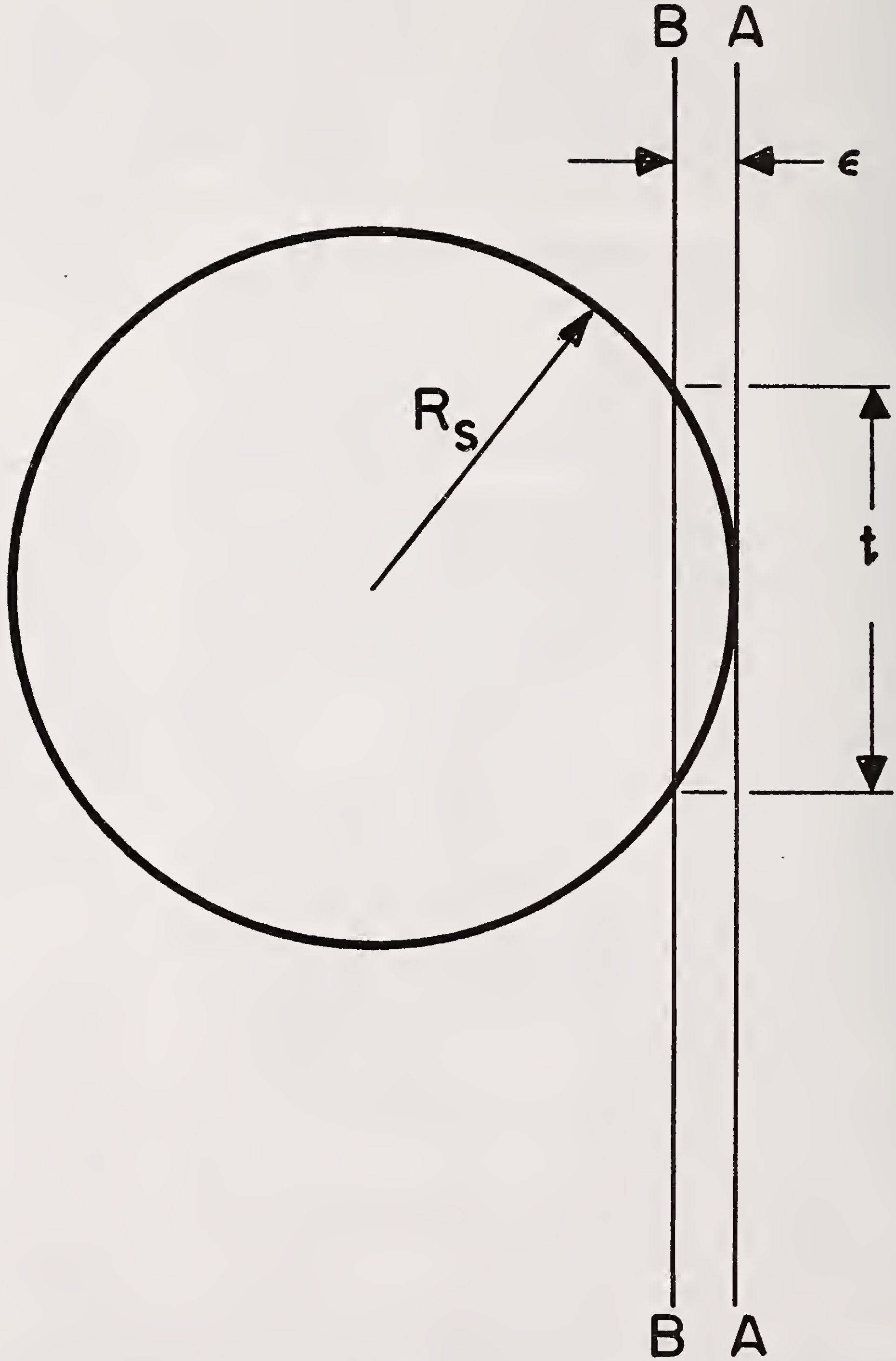

Figure 5. Illustration of slit-edge penetration effects.

The opening of each slit pair is monitored by a Moiré fringe counter which consists of a precision-ruled grating attached to one cylinder and a readout head attached to the other [6]. The readout head counts the rulings which pass it with a least count of 0.0001 inches. The accuracy is $\pm$ 0.0001 inches, established by comparing the fringe counter readout with gauge block measurements. The Moiré fringe counters measure the slit openings to within a constant since they have arbitrary, resettable zeros. Reference positions for each slit are established by electrically sensed limit switches whose positions correspond to apertures of approximately 0.020 inches horizontally, and 0.030 inches vertically. Reproducibility of the reference positions is established by setting the counter readings to zero with the slits at their reference positions. The slits are opened, adjusted a number of times, and eventually returned to the reference positions. The resulting readout is nearly always within $\pm$ 0.0002 inches of zero, even after several days.

To determine the true aperture openings, the openings which correspond to the reference positions of the slits must be measured. We do this by measuring the counting rate for elastic electron scattering as a function of slit opening, as given by the fringe counters. The openings at the reference positions are determined by extrapolating to the counter reading which produces zero count rate. With counting-rate loss and small background corrections directly measured by the detector system, the extrapolation is found to be linear provided that, for the horizontal aperture, the slits are opened symmetrically about the reference position. A typical single determination of a reference opening to a standard deviation of 0.0003 inches can be made in about 15 minutes.

Finally, we note that an optical determination of the scattering geometry is valid only in the absence of the stray magnetic field in the region between the target and the aperture slits. Our aperture slits are well outside the spectrometer magnetic field. The stray field near the slits is $\lesssim 3 \times 10^{-3}$ of the central field in the magnet. Based on this value and taking account of the symmetry of the field about the spectrometer midplane, we can show that the stray field effect on scattering angle and solid angle is completely negligible: less than 10^{-4} on solid angle; less than 10^{-3} degrees on scattering angle.

C. Target Support Assembly

The target support assembly shown in figure 6 serves many functions besides simply holding targets in the beam near the axis of rotation of the spectrometer. Ten inches of vertical motion is available so that several targets can be placed in the beam alternately without opening the vacuum system. Vertical oscillation with typically 1/4 inch travel, or horizontal oscillation with 1/2 inch travel and variable speed, or both simultaneously, is available to reduce local heating of targets by the beam. The horizontal drive mechanism also operates the target location beam profile scanners. Rotational motion, which is fitted with a high-precision readout, allows selection of target angles.

The target support base is bolted and grouted to the floor of the room independently from the spectrometer. Leveling and translating adjustments are provided in order to bring the rotation axis of the target assembly into coincidence with the spectrometer rotation axis. The devices which make these adjustments are omitted from figure 6 for the sake of clarity. The base, the scattering chamber baseplate, the two vertical support columns which connect them, and four guide rods constitute the stationary part of the target assembly. A stepping motor drives a jackscrew to provide vertical motion, and a multiturn potentiometer which serves as the sensing element of the servo system that controls vertical target motion. This servo provides vertical positioning reproducible to better than 0.004 inches.

The movable part of the assembly rides on ball bushings which run on the guide rods. These ball bushings are fixed to the jacking flange and the bellows flange shown in figure 6. These two members are rigidly connected to form a stable, vertically moving platform for the rest of the assembly. The motors, gear trains, potentiometer, limit switches, etc., which provide the rotation and horizontal oscillate motions are omitted from figure 6 for clarity; however, the driveshafts for these motions can be seen protruding below the bellows flange. Vacuum-tight connection between the moving and stationary parts of the target assembly is provided by a large bellows. Rotation and oscillation drives are carried into the evacuated part of the system by a pair of rotary feedthroughs.

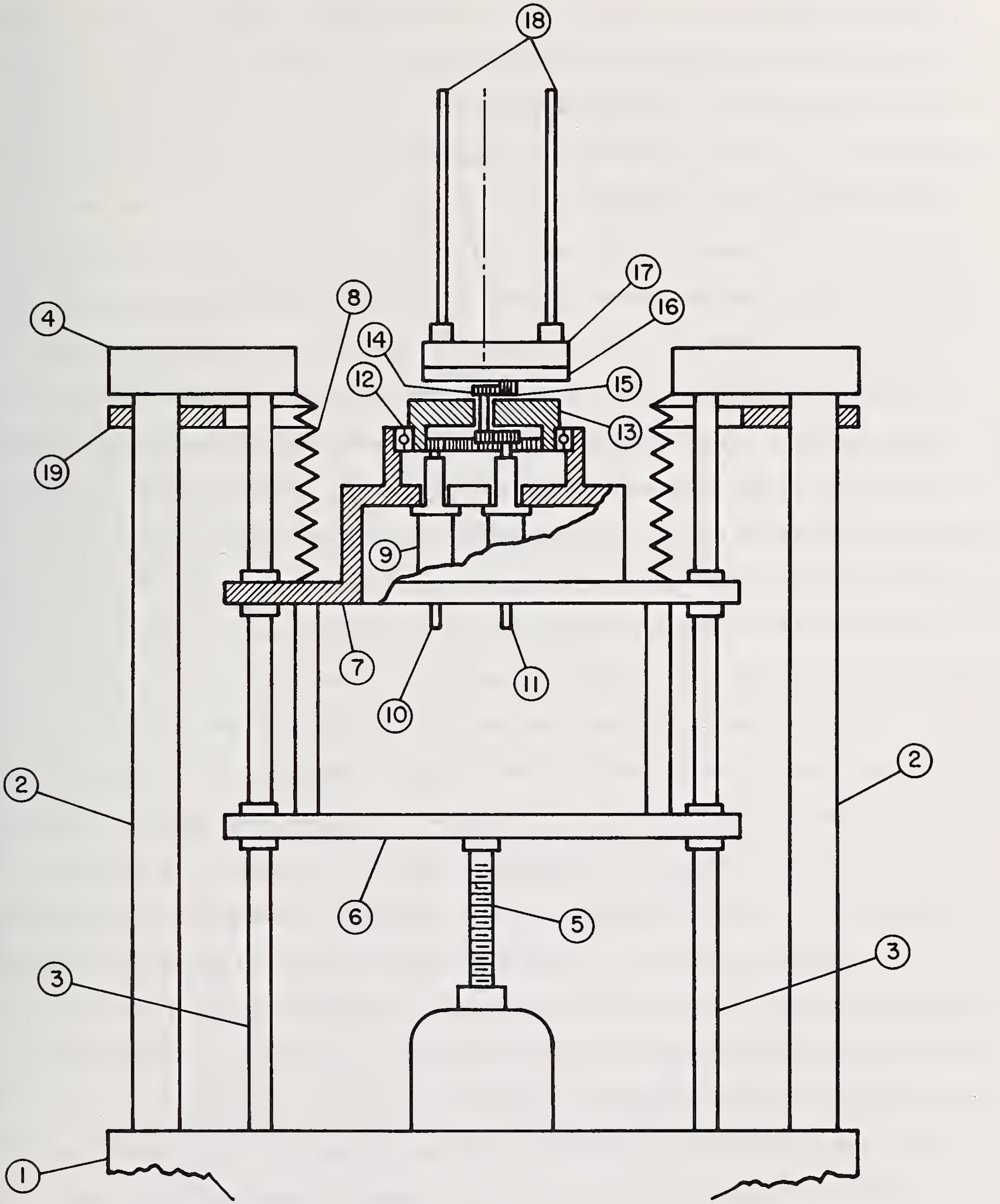

Figure 6. Target Pedestal Assembly. The components are: (1) base, (2) support column, (3) guide rods, (4) scattering chamber baseplate, (5) jackscrew, (6) jacking flange, (7) bellows flange, (8) bellows, (9) rotary feed-thrus, (10 rotation driveshaft, (11) oscillation driveshaft, (12) turntable bearing, (13) turntable, (14) linear cam, (15) idler wheel, (16) translation stage, (17) target platform, (18) target ladder roads, (19) indicator ring.

A pinion gear driven by one of the rotary feedthroughs engages a ring gear fixed to the rotating turntable. The rotational motion is guided by a high quality ball bearing. Great precision is needed in all components of the rotation mechanism to insure that the external readout, a ten-turn potentiometer, tracks the angle of rotation of the target. The standard deviation of the readout is 0.08 degrees.

The second rotary feedthrough drives the horizontal translational motion through a reduction gear pair. The driven gear is fixed to the lower end of a shaft which passes through the rotating turntable on its axis of rotation. This shaft is guided by two ball bearings (not shown in figure 6) mounted in the turntable. The upper end of the shaft holds a linear cam which pushes against an idler wheel mounted to the moving part of the translation stage. The remainder of the translation mechanism, which is omitted from figure 6 for clarity, consists of two parallel rods fixed to the turntable, and two ball bushings which are fixed to the translation stage and ride on each of the rods to provide a smooth horizontal motion so that the target platform remains at a fixed angle during horizontal oscillation. A spring is used to keep the idler wheel in contact with the linear motion cam. Note that when the turntable rotates, the idler wheel moves around the cam. Thus in normal use, horizontal translational motion accompanies rotation. A purely rotational movement of the target platform is obtained by disengaging the idler wheel from the cam and clamping the translation stage to the turntable. The horizontal translation motion is driven by a stepping motor. Exactly 400 steps are needed to produce one full revolution of the cam. Two hundred steps drive the translation stage from one extreme of its travel to the other and the next 200 steps return the stage to the original position. Except near the turn-around points, the motion is extremely linear, producing a displacement of (0.00283 $\pm$ .00003) inches per step. The motion is also highly reproducible, such that upon repeated traverses through 400-step cycles, the ladder returns to the same position within 0.0005 inches standard deviation. The horizontal translation mechanism provides the motion needed for the target-location beam-profile scanners described in section II D.

The uppermost portion of the target support assembly consists of the target platform and target ladder rods. The rods are precision-ground 1/2-inch diameter stainless steel, extending eleven inches above the platform. Targets mounted in holders are stacked on the ladder rods. The holders, shown in figure 7, position thin foil targets within 0.001 inches of the target plane, defined to be the plane of the axes of the two ladder rods. The ladder rods must be coplanar, but they need not be accurately parallel within this plane. It is highly desirable that the target plane contains the axis of rotation of the turntable, and that this axis be vertical. More precisely stated, the axis of rotation should be accurately parallel to the direction of "vertical" motion of the target ladder. By means of a series of measurements and adjustments, we have been able to achieve these conditions to a high degree of accuracy. The measurements are described in section IV. After final adjustment, all critical parts are held in precise alignment by ground steel dowel pins. Thus disassembly for servicing is possible without changing the alignment.

The target support assembly is not completely rigid when subjected to horizontal forces, which occur during vacuum system pumpdown, changing of beam line plumbing (other experiments use the same beam line), and coupling or uncoupling of the spectrometer to the scattering chamber ports. To facilitate repositioning the target support assembly when it does move, an indicator ring is fitted to the underside of the scattering chamber baseplate. This ring consists of an 18-inch diameter cylindrical disc whose outer surface is, for all practical purposes, a perfect circle. The ring was initially aligned concentrically with the target platform axis of rotation by the method illustrated in figure 8. A dial gauge is rigidly supported from the target platform so that its plunger points radially inward, engaging the outer surface of the indicator ring. Dial gauge readings are taken while the target platform is rotated. The indicator ring is repositioned and the readings repeated until the dial gauge reading does not change with rotation. The indicator ring is then pinned in position and a final set of dial gauge readings as a function of angle of rotation are taken. We achieved a total indicator reading (difference between largest and smallest value) of 0.0010 inches. Because the target axis of rotation is not perfectly parallel to the direction of vertical target motion, this concentricity holds exactly only when the vertical target position is at a particular reference setting. The reference setting used for this measurement, referred to as target position No. 5, places a standard BeO beam-viewing bullseye at beam height. Note that these concentricity measurements can only be made when the target translation stage motion is disengaged.

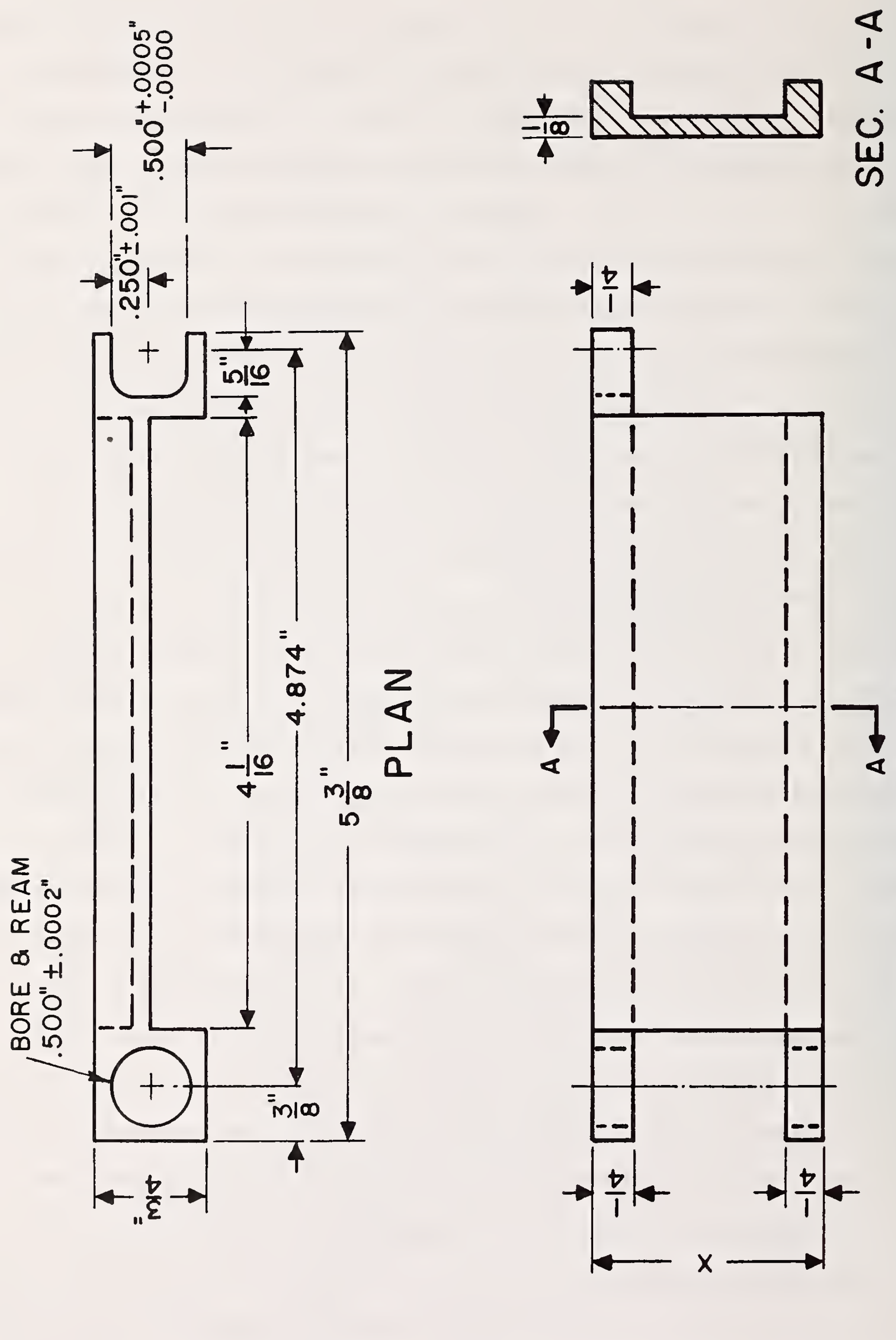

Figure 7. Target Holder Blank. An appropriate hole is cut in the blank to permit passage of the beam. The size and shape of the hole, and dimension x depend on the dimensions of the target foil. A retaining frame (not shown) presses the target foil against the flat surface of the blank. The frame, foil, and holder are assembled with small screws around the periphery of the foil.

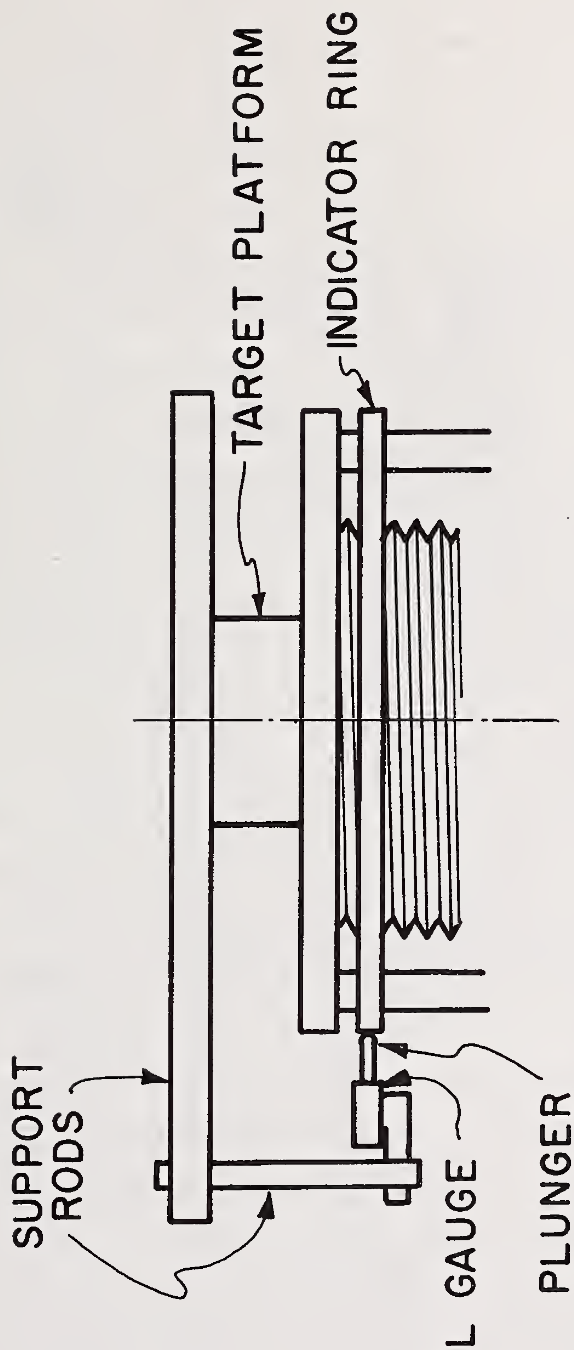

Figure 8. Procedure for aligning the indicator ring.

The indicator ring, first used to place the target rotation axis in coincidence with the spectrometer rotation axis, allows the target assembly to be returned to the same location when necessary. The method employed to measure indicator ring location is illustrated in figure 9. Four dial gauges (A, B, C, D in the figure) contact the indicating ring radially at 90° intervals around its periphery. These gauges are supported on a common rigid framework fastened to heavy webs which are integral members of the rotating part of the spectrometer base. Thus, these dial gauges rotate with the spectrometer, but do not share its radial motion. The target support assembly is placed at the center of rotation of the spectrometer by translating the support assembly in order to minimize the changes of readings of all four dial gauges with respect to spectrometer angle changes. The readings taken at the final position of the target assembly as a function of spectrometer angle are displayed in figure 10 and Table I. In this figure and table, only the difference readings between diametrically opposed pairs of gauges are given, since any motion of the indicating ring relative to the dial gauges produces equal magnitude, opposite sign changes in the readings of the two opposed gauges. The use of opposed pairs reduces measurement errors caused by effects like imperfections in the indicator ring surface, changes in dimensions of the structure due to thermal expansion, etc. Note that if the indicator ring is moved a distance X along the D-B axis (for example), the value of (D-B) will change by 2X. In figure 10, the values of (D-B) and (A-C) readings are plotted. Five complete independent sets of data were taken, allowing a determination of the variance of the measurements. Since the average values for the data at each angle have standard deviations of 0.0011 inches, the angle dependences shown in figure 10 are real effects. If these dependences were due to the indicator ring not being concentric with the axis of rotation, the curves in figure 10 would be sine waves with a period of 360°, identical amplitudes, and a 90° phase difference between D-B and A-C readings. This is clearly not the case. The most reasonable explanation of the observed angular dependences is that they are caused by imperfections in the main bearing which guides the spectrometer rotation. These effects do not influence our ability to determine the scattering geometry, provided that the position of the spectrometer in space at any given scattering angle is reproducible. The indicator ring dial gauge measurements show that the axis of rotation of the spectrometer,

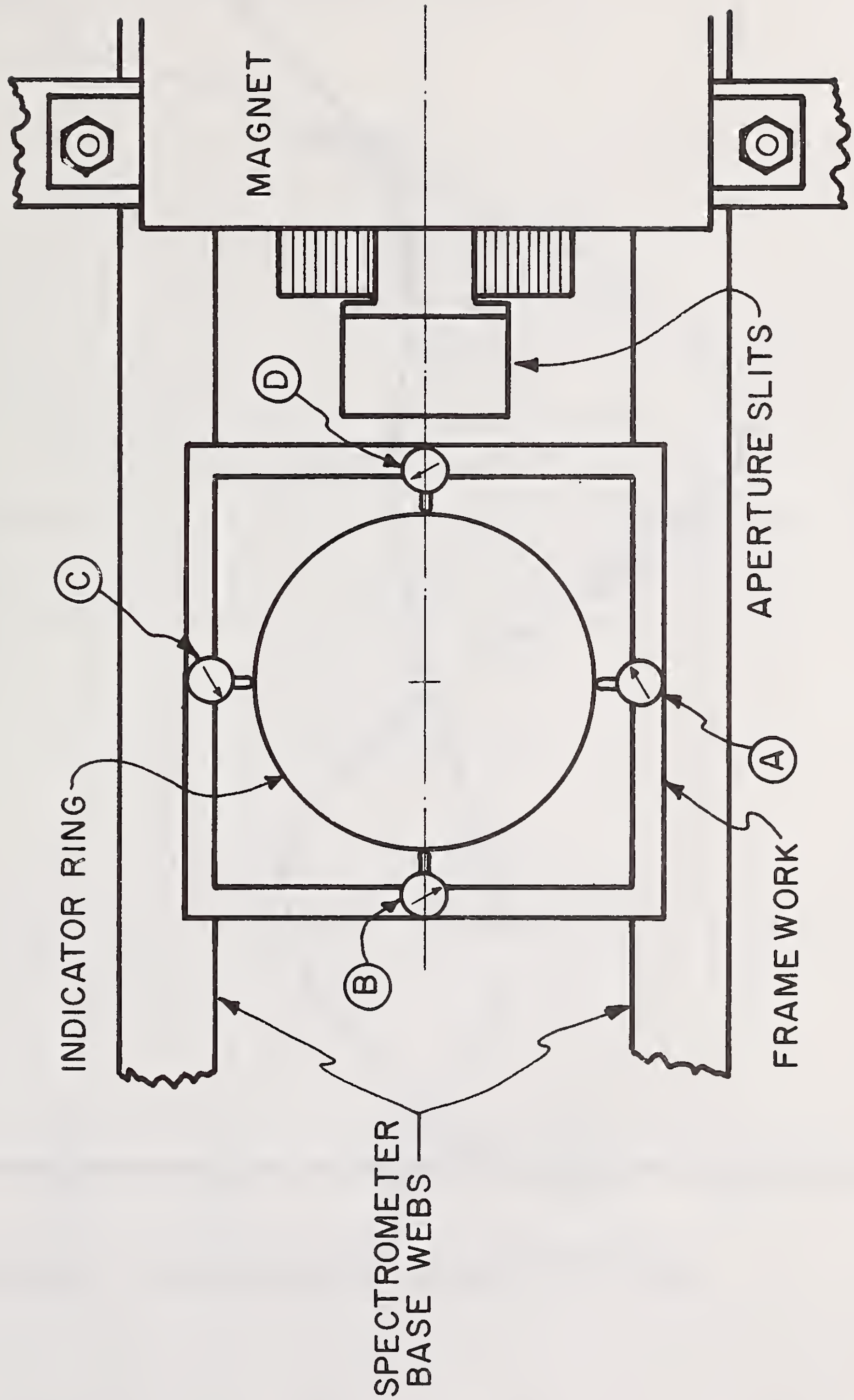

Figure 9. Plan view showing the location of the indicator ring dial gauges A, B, C, and D.

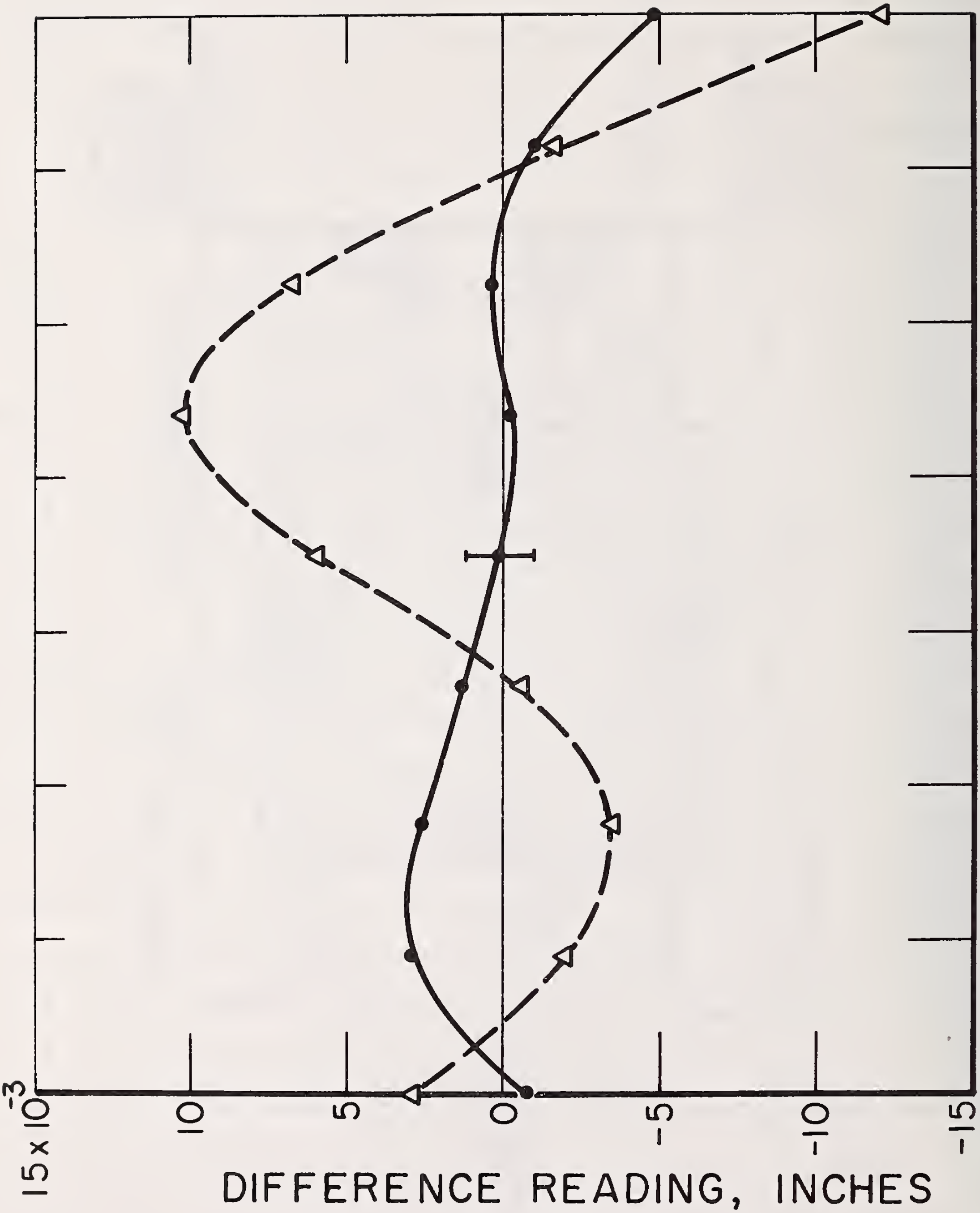

Figure 10. Indicator ring dial gauge readings as a function of spectrometer angle. Circles are values of D-B, triangles are values of A-C. Data are from Table I, with the average value subtracted. The standard deviation for each plotted point is indicated by the flags on the D-B point at 110 degrees.

at a fixed scattering angle is reproducible to $\pm 1.1 \times 10^{-3}$ inches (standard deviation) in each horizontal direction. The influence of this variation on the accuracy of scattering angle determinations will be discussed further in section VI.

D. Beam Profile Scanners

Four profile scanners are needed to measure the spatial and angular distribution of the electron beam incident on a scattering target. The scanners all operate on the same principle, as illustrated in figure 11, but differ from each other in detail. A horizontal beam profile is obtained by having a vertical sensing rod move across the beam in the horizontal direction as shown in figure 11a. The sensing rod can be any device which produces an output signal proportional to the current, I, striking the rod. The profile is this current as a function of the rod position, x, as shown in figure 11b. The scale factor and initial position of the rod must be known. Fine details of the beam profile are not needed in order to measure cross sections to the desired accuracy. It is sufficient to determine the beam centroid location, $\bar{x}$, and root-mean-square width w, which are defined by

$$\bar{x} = \int I(x)x dx / \int I(x) dx \qquad (1)$$

and

$$w = [\int I(x)(x - \bar{x})^2 dx / \int I(x) dx]^{1/2} . \qquad (2)$$

Note that the current I(x) is an integral of the beam current density J(x,y) over the transverse direction. That is

$$I(x) = \int J(x,y) dy . \qquad (3)$$

It is clear from the form of eq (1) and (2) that the constant of proportionality between the sensing signal and actual current is irrelevant. A reasonably linear response is needed.

The upstream beam scanners are needed to determine the direction and angular size of the beam incident on the target. Two scanning devices, for measuring horizontal and vertical profiles, are mounted in a common chamber. Figure 12 is a cross sectional view of the horizontal upstream scanner. The sensing element is a 1/8-inch diameter glass rod, used as a Cerenkov detector. Light generated by the electron beam is guided along

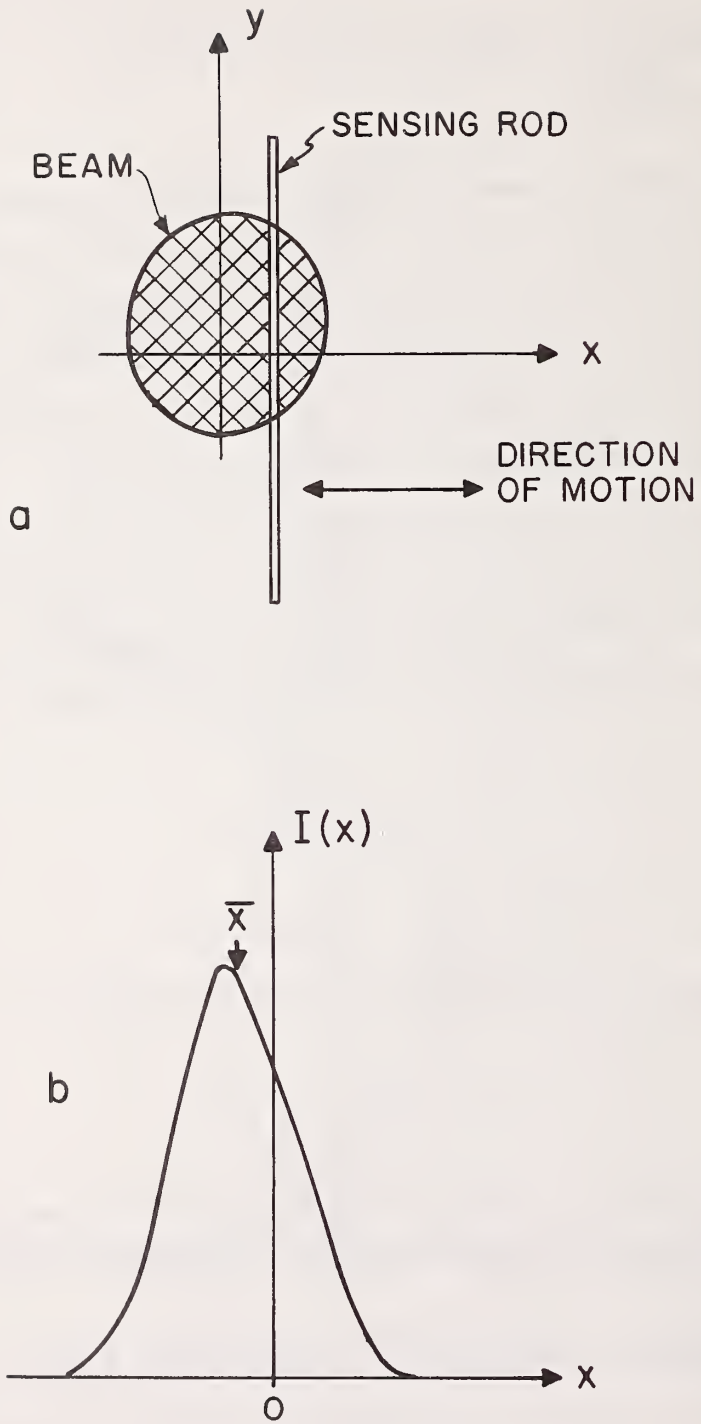

Figure 11. Operation of beam profile scanners
a. Cross sectional view of beam with sensing rod.
b. Current striking the sensing rod as a function of its position x. $\bar{x}$ is the beam centroid location.

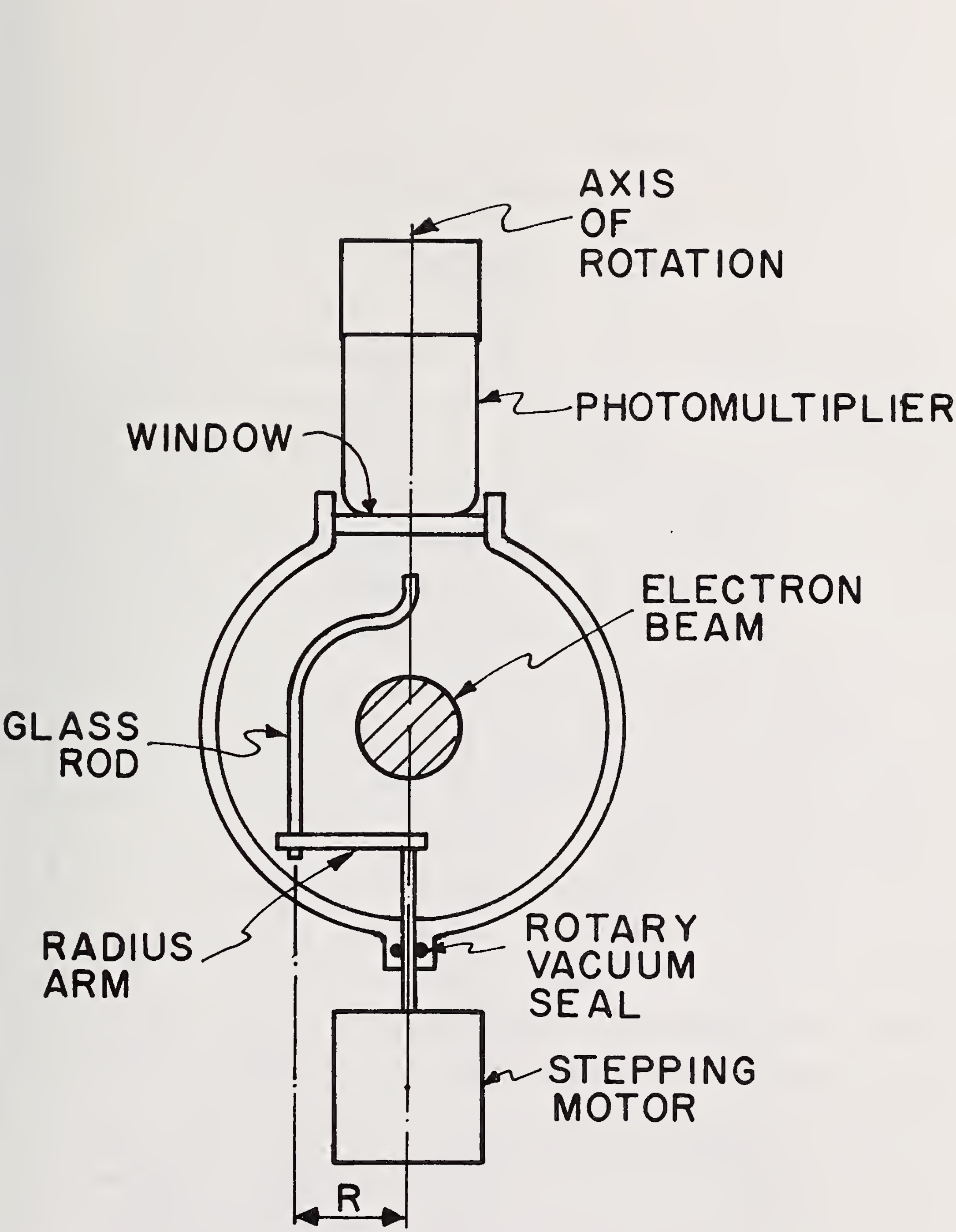

Figure 12. Upstream beam profile scanner.

the rod and emitted from its end, in the direction of the photomultiplier tube. The rod is bent so that its free end is on the axis of rotation, in order that the light intensity seen by the phototube be independent of the position of the rod. The sensing rod is driven by a stepping motor to produce a rotary motion with radius ρ. The step size is (1/200) of a revolution. Thus, the transverse coordinate, x_R, of the rod is given by

$$x_R = \rho \sin \frac{(N - N_o)\pi}{100} , \tag{4}$$

where N is the number of steps taken. N_o defines the starting position so that $x_R = 0$ on the axis of rotation. The stepping motor is driven in synchronism with the linac pulse repetition frequency, one step per beam pulse. The photomultiplier output signal due to each beam pulse is integrated, digitized, and stored in the on-line computer as a function of the step number N. After one revolution, the computer gates off the pulse train which drives the stepping motor, and analyzes the spectrum obtained. This spectrum has two peaks; one obtained when the sensing rod passed through the beam moving toward the right, the other when the rod was moving toward the left. Both peaks are needed in the analysis because the starting position, $N_o = (50 \pm 5)$ steps, is not accurately known. Computer analysis of the two-peaked spectrum eliminates the dependence on N_o, and yields $\bar{x}$ and w employing eq(1) and (2) (converted to discrete sums instead of integrals). A single measurement of this type locates the beam centroid with a standard deviation of about 0.4 steps, corresponding to an uncertainty in beam direction of $\pm$ 0.9 x 10^{-4} radians ($\pm$ 0.005 degrees).

The current sensing element of the target location beam scanner is a thin wire operating as a secondary emission monitor. The wire is mounted in a target holder frame as shown in figure 13. A flexible lead connects the sensing wire to a feedthrough mounted in one of the scattering chamber ports. The signal is amplified by a charge-sensitive amplifier and is read into the on-line computer system through an analog-to-digital converter, as described above for the upstream scanners. The same readout system is used for both horizontal and vertical profile measurements, the only difference being that the target ladder height is changed to put the appropriate sensing wire at beam elevation. Both horizontal and vertical profile measurements are obtained by horizontal oscillation of the target holder. As in the case of the upstream scanners, motion is produced by a

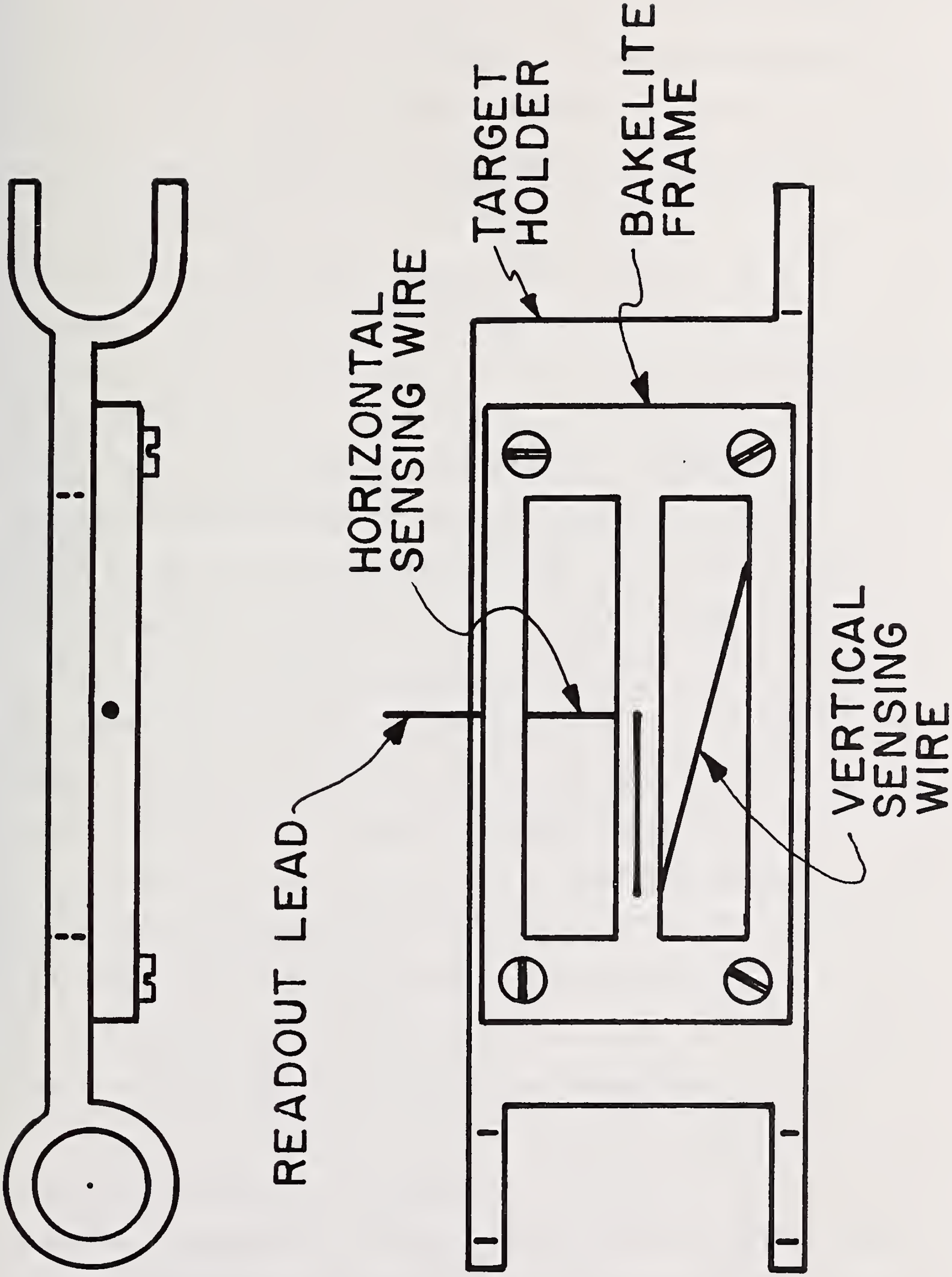

Figure 13. Target location beam scanners.

stepping motor driven synchronously with the beam repetition frequency, the only differences being that in this case the motion is linear rather than sinusoidal and 400 steps are required to complete one cycle of motion. The position scans are analyzed by the computer in the manner previously described, again using the left-going and right-going portions of the scan to eliminate the need for accurate knowledge of the starting position.

The position of the horizontal scanning wire in the direction transverse to the beam axis is

$$x_B = [x_o + (N - N_o)\Delta] \cos \theta_T - z_o \sin \theta_T, \tag{5}$$

where θ_T is the target angle,

Δ is the step size (.00283 ± .00003 in.),

and x_o and z_o are the coordinates of the wire in the holder.

Here we use $N_o \simeq 100$ steps. Since x_o and z_o are not accurately known, a priori, they must be determined by calibration. The calibration procedure consists of measuring a beam centroid position at several values of θ_T. A typical set of measurements consisting of four scans at each of three angles, θ_T, will determine x_B, x_o, and z_o to within standard deviations of .0016, .008, and .0025 inches, respectively. After calibration, subsequent determinations of x_B can be made without changing θ_T. Note that this procedure determines the transverse beam centroid position with respect to the axis of rotation of the target assembly.

Vertical beam profile measurements use the inclined sensing wire shown in figure 13. The height, h, at which this wire intercepts the horizontal centroid of the beam (x_B) is given by

$$h = h_o + S \left[\frac{x_B}{\cos \theta_T} + z_v \tan \theta_T - (N - N_o)\Delta \right], \tag{6}$$

since this sensing wire lies in a plane which is parallel to the plane defined by the centers of the target ladder rods, and displaced from it by a distance z_v. The symbols in eq (6) not previously defined are S (= 0.25), the slope of the inclined wire to the horizontal direction and the constant h_o. The value of z_v can be determined by measurements at different settings of θ_T, as in the case of the horizontal scanner, but there is no analogous "internal" method for determining h_o. Fortunately, the beam height can be adequately determined by using the bullseye beam viewer (estimated accurate to <0.02 inches.)The vertical beam scanner is used only to measure changes in beam height occurring during data taking, and the beam size. The standard deviation of a single measurement of relative beam height is typically 0.002 inches.

III. System Geometry

In this section we will define the quantities which specify the scattering geometry. We employ a coordinate system whose X and Z axes, and origin "0," are shown in figure 14. The Y axis of this coordinate system points out of the plane of the figure, and vertically upward in space. This coordinate system rotates with the spectrometer, since its Z axis bisects the line joining the centers of the cylinders which define the horizontal spectrometer aperture (at point Q).

The origin point (0 in figure 14) is chosen to be a fixed point in space, although neither the target support assembly nor the spectrometer axis is rigidly fixed in space. The point 0 is established by finding a point on the axis of rotation of the target turntable, at nominal beam height, with the target support assembly in its reference position. The reference position is obtained at the vertical target setting #5 defined previously, and with the indicator ring dial gauges at the values listed in Table I. During the calibration, the location of point 0 in the horizontal plane was established to well under 10^{-3} inches. However, since the target assembly was moved, the original position can be reproduced only to within $\pm$ 0.0011 inches in each horizontal direction as already discussed in section II.

We next define a baseline, shown in figure 14 by line OB, along the incident beam direction. The second fixed point needed to define the baseline is the geometrical center of the exit flange of the vacuum pipe fixed in the quadrupole magnet shown in figure 1. This point is only needed to define the baseline direction in the X-Z plane, since this plane is horizontal by assumption.

Once the baseline has been established, the calibration of the scattering angle scale consists of determining the angle, θ_o, between the baseline and the Z axis. We measure θ_o at nine reproducible positions, established by fiducial blocks permanently mounted on the fixed base of the spectrometer. One of the fiducial positions corresponds

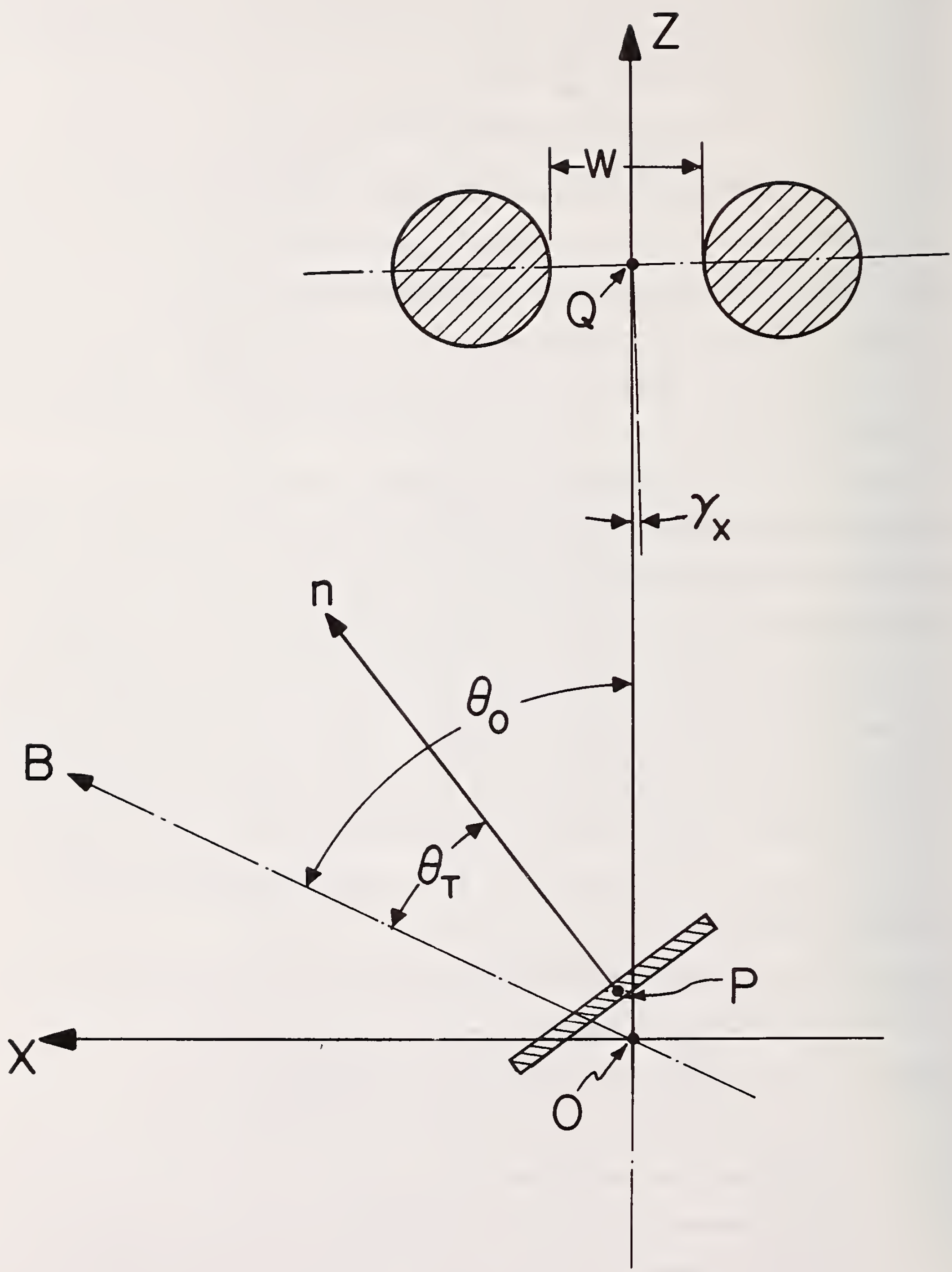

Figure 14. Coordinate system used in this report, in plan view. The shaded circles represent the horizontal aperture slits. The shaded rectangle represents a target oriented in transmission geometry. The line B indicated the beam direction.

to $\theta_o = 180°$; that is, the point Q in figure 14 is (very nearly) on the baseline OB. The other eight fiducial positions correspond to scattering angles at which the spectrometer aperture is aligned with the scattering chamber ports. The angular position of the rotating spectrometer base can be set at any of the fiducial positions, to within 3×10^{-4} degrees, by observing the reading of a dial gauge mounted on the rotating base, as shown in figure 15. Scattering angles differing from a fiducial position by $<0.4°$ are determined with the aid of the reading of this azimuthal dial gauge. In addition to depending on the azimuthal dial gauge reading, the scattering angle is a function of the spectrometer's radial position because of the transverse motion accompanying radial motion, as described in section II and displayed in figure 3.

In order to locate the spectrometer aperture in the horizontal plane, the distance OQ, the aperture, W, and the angle, γ_x, must be known. The distance OQ, hereafter called L_x, is a function of the spectrometer's radial position and depends weakly on θ_o because the spectrometer motion about O is not a pure rotation. γ_x, defined as the angle between the line joining the centers of the aperture cylinders and the Z axis, is positive in the direction shown in figure 14. W, measured in the direction joining the centers of the aperture cylinders, is perpendicular to the Z axis only if $\gamma_x = 0$. As described in section IIB, W = 0 is defined from an extrapolation to zero count rate which, in general, does not exactly coincide with the point at which the cylinders make physical contact.

The location of the vertical spectrometer aperture shown in figure 16 is defined by the distance L_y, opening H, and angle γ_y, analogous to L_x, W, γ_x for the horizontal case. Additionally, the vertical distance y_A must be known.

The point at which the incident electron beam strikes the target is measured by the profile scanners relative to the fixed point P and angle θ_T, indicated in figure 14. P is the intersection of the axis of rotation of the target pedestal and the X-Z plane. The angle, θ_T, between the baseline direction B and the normal, n, to the target plane, is positive in the sense shown in figure 14.

O and P, indicated in figure 14 to be different points, were coincident when the geometry calibration was performed. P is slightly displaced from O if the vertical target position is different from its reference position or if the indicator ring, and

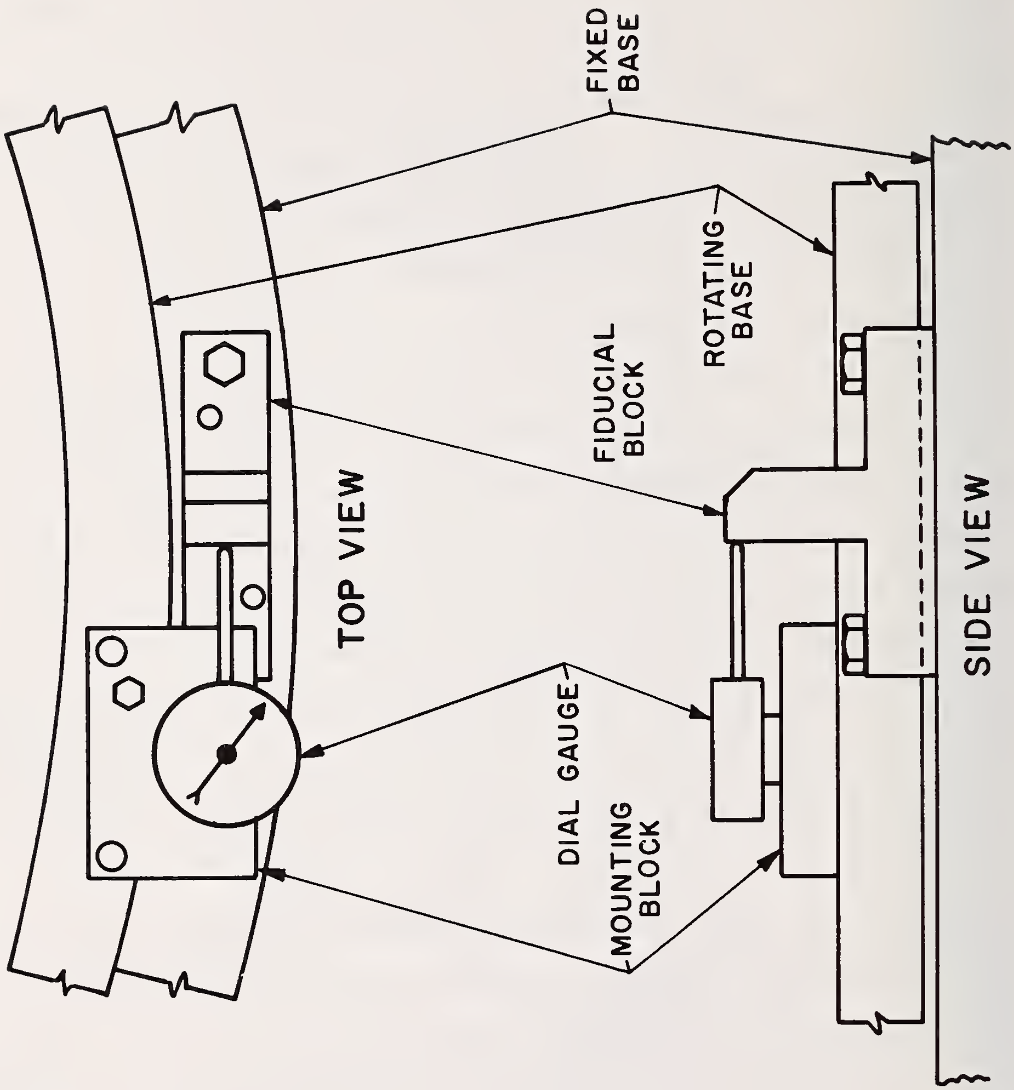

Figure 15. Azimuthial dial gauge mounted on the rotating base of the spectrometer and indicating on one of the fiducial angle blocks. The dial gauge and its mounting block are removed from the rotating base to allow rotation of the spectrometer. Alignment pins insure accurate repositioning.

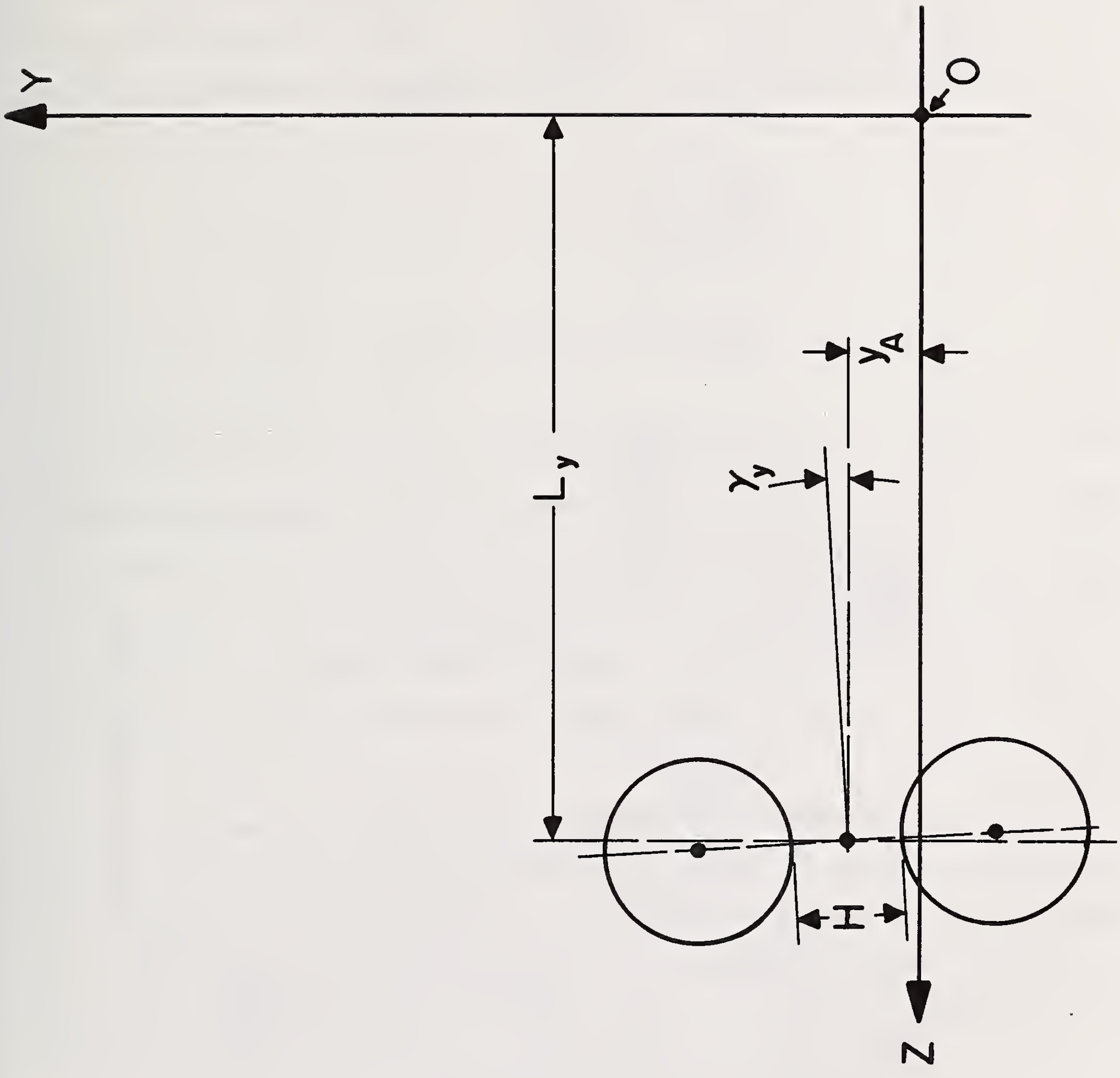

Figure 16. Coordinate system used in this report. In this view the X-axis is perpendicular to the plane of the figure. The circles at the left side of the figure represent the vertical aperture slits.

therefore the target assembly, is not at the position defined by the values of D-B and A-C in Table I.

In section II, we described the measurement of beam position relative to the axis of rotation by means of the beam profile scanners. Note that x_B, defined by eq (5), is measured perpendicular to the baseline OB, which is not in the X direction of the coordinate system defined by figure 14 unless $\theta_o = 0$. The target point coordinates x_T and z_T are given by

$$x_T = \frac{x_B}{\cos\theta_T} \cos(\theta_o - \theta_T) + \eta \sin(\theta_o - \theta_T) + x_P,$$

and (7)

$$z_T = -\frac{x_B}{\cos\theta_T} \sin(\theta_o - \theta_T) + \eta \cos(\theta_o - \theta_T) + z_P .$$

In eq (7), x_P and z_P are the coordinates of point P, and η is the displacement of the target point from the target plane (which passes through P). The positive direction of η is in the direction of the normal n. For target holders constructed as shown in figure 7, the maximum value of η is the target-foil thickness.*

The vertical distance, h, of the target point from the origin, O, can normally be neglected since $|h| \lesssim 0.02$ in., but the vertical displacement of the slit assembly, y_A, cannot.

The last quantity needed to define the scattering geometry is the actual direction of the incident electron beam. The projection into the horizontal plane of the angle between the baseline and the actual beam line is shown as α_X in figure 17. In this figure, the points O and P, and the axes labeled B and Z are the same as in figure 14, and T is the point where the beam intersects the target plane. In terms of measurable quantities,

$$\alpha_X = \frac{x_B + x'_P - (x_R + x_C)}{B_X} , \tag{8}$$

---

* Some target holders have been prepared with a recess which limits η to $\pm$ (one-half of the target foil thickness), and makes the average value of η zero.

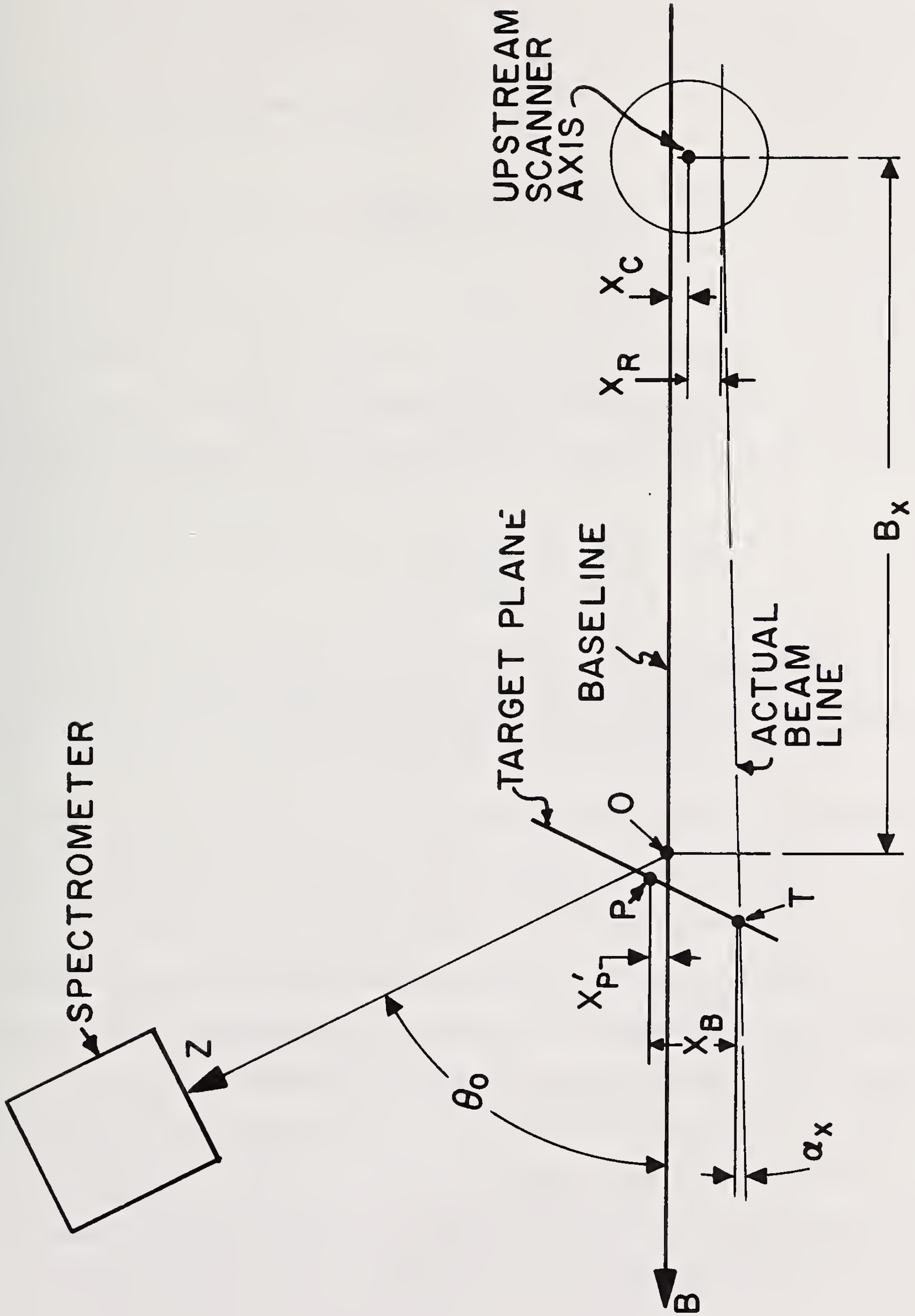

Figure 17. Definition of quantities measured relative to the baseline. Plan view. The electron beam goes from right to left in this figure along the line marked "B".

where x_C is the transverse coordinate of the axis of the horizontal upstream beam scanner,

x'_P is the projection, in the horizontal direction perpendicular to the baseline, of the distance OP, and

B_X is the distance between the axis of the horizontal upstream beam scanner and the origin point 0.

The small angle approximation used here is adequate since $|\alpha_X| \lesssim 10^{-3}$ radians and the projection on the baseline of the distance OT is negligible ($\sim$0.1 in. compared to $B_X \simeq$ 100 in.). All quantities on the righthand side of eq (8) are positive in the directions indicated in figure 17, except for x'_P, which is negative as shown. For completeness, we also define the angle, α_Y, of the beam line projected into the vertical plane, although its effect on a cross section determination is extremely small. The appropriate analog of eq (8) is

$$\alpha_Y = \frac{h - (y_R + y_C)}{B_Y} , \tag{9}$$

where y_R, y_C, and B_Y are exact analogs of x_R, x_C, and B_X, respectively. The distances h, y_R, y_C are measured from the horizontal plane passing through 0, with the positive direction upward.

With the geometry fully defined, we can now explicitly state how the effective solid angle Ω_{eff}, and the effective scattering angle, $\overline{\theta}$, are determined. An electron incident on the target along the direction defined by α_X and α_Y scatters from a target nucleus located at (x_T, h, z_T) through polar angle θ, at an azimuthal angle ϕ. The solid-angle integral of eq (1) is to be performed over the range of (θ,ϕ) allowed by the positions of the aperture slits. The integration limits are thus functions of x_T, h, z_T, α_X, α_Y, θ_o, W, H, L_X, L_y, γ_X, γ_y, y_A, and R_S.* Of these, all but the first five are constants for any one cross section measurement. However, x_T, h, z_T, α_X, and α_y are distributed variables because of the angular and spatial spread of the beam as well as the range of scattering centers in the target, represented by the variable η. We can write

---

* There is also a dependence on the angle of multiple scattering in the target which will not be discussed here except to note that this effect can be accounted for by modifying α_X and α_y appropriately.

$$\int_{\text{aperture}} \sigma(E,\theta)d\Omega = \sigma(E,\overline{\theta})\cdot\Omega_{eff} , \qquad (10)$$

where the integration limits depend on all of the geometrical parameters, including appropriate averaging over the values of distributed variables. To obtain a Taylor's series expansion of the cross section, we define

$$S_n(\theta_1) = \frac{1}{n!\sigma(E,\theta_1)} \frac{\delta^n\sigma(E,\theta_1)}{\delta(\cos\theta)^n}\Bigg|_{\theta=\theta_1} \qquad (11)$$

Then

$$\Omega_{eff} = \sum_{n=o}^{oo} S_n(\theta_1) \int_{\text{aperture}} (\cos\theta - \cos\theta_1)^n d\Omega . \qquad (12)$$

We have written a computer subroutine which computes

$$P_n(\theta_1) = \int_{\text{aperture}} (\cos\theta - \cos\theta_1)^n d\Omega , \qquad (13)$$

for as many values of n as needed, for any value of θ_1, when the 14 geometrical parameters* listed above are supplied as input. Averaging over the distributed variables is performed by Monte-Carlo methods. A convenient definition of $\overline{\theta}$ is that value of θ_1 which makes P_1 identically zero. For reasons of numerical accuracy, we obtain $\overline{\theta}$ from the relation

$$\cos\overline{\theta} = \cos\theta_o + \frac{P_1(\theta_o)}{P_o} . \qquad (14)$$

The experimental geometry also enters into the determination of W_o, the number of target nuclei per unit area normal to the beam direction. For a uniform-thickness plane target only θ_T, α_X, and α_y are needed to determine W_o. The dependence on α_y is negligible, and the dependence on α_X is always slight.

---

* The number of input parameters is reduced to 13 since h and y_A enter only in the combination $h - y_A = y_T$.

In this section we begin a description of the alignment and calibration of the apparatus, the order being approximately chronological so the dependence of each step on the preceding ones can be seen. The first step is to align and calibrate the target support assembly so that its axis of rotation can be utilized as the geometric origin.

The first step in aligning the target pedestal is to establish the relative orientation of the target plane, axis of rotation, and the directions of vertical and horizontal motion of the target platform. The measurements about to be described had to be repeated several times, adjusting the orientation of the components each time, until the alignment was judged to be satisfactory. Only the final set of measurements will be described. Figure 18 shows how the measurements are performed. A target holder blank mounted on the ladder rods provides a solid surface in the target plane, R_1. (By definition, the target plane is the plane containing the axes of the ladder rods.) A dial gauge, mounted at nominal beam height, has its plunger in contact with this surface. The line through 0 labeled "A" is the axis of rotation of the target turntable. The angle between R_1 and A is defined to be β. Note that R_1 does not necessarily pass through 0; in fact, the horizontal distance, p, between 0 and R_1 is the quantity measured by the dial gauge. Rotating the turntable through 180°, (i.e., $\theta_T \rightarrow \theta_T + 180°$), moves the target plane to the position indicated by the line R_2, still at angle β with respect to A, but in the opposite direction. In order to measure p in this orientation, the target blank must be reversed on the rods. The direction of vertical motion of the target platform is indicated by the line "Y" in figure 18. The projection of the angle between Y and A into the plane of the figure is δ. Lowering the target pedestal a distance V from the reference position causes the ladder plane to lie along the line R_3, which is parallel to R_1. In order to remain at the same height in the room the target blank must be moved up the ladder rods by the same amount (V), thus moving the blank toward the dial gauge and increasing p. The dial gauge can be mounted at any azimuthal angle θ_o. Final data were taken at $\theta_o = 180°$ and 270°. For each of these values of θ_o, we measured p at seven values of V over a range of about 7 inches, both with $\theta_T = \theta_o$ and with $\theta_T = \theta_o + 180°$. A least-squares fit to the data with the equation

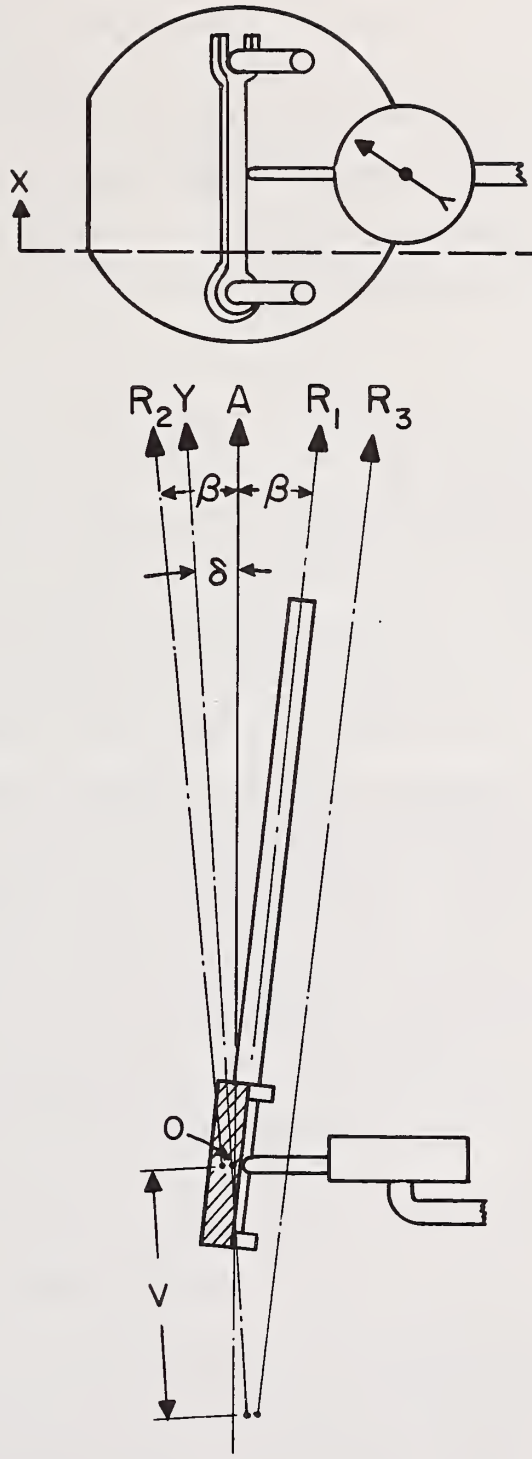

Figure 18. Target ladder, illustrating the method for measuring the alignment of the ladder with a dial gauge. A is the axis of rotation of the turntable. R_1 is the plane of the target ladder rods. A 180° rotation of the turntable puts this plane in the direction indicated by R_2. Y is the direction of "vertical" motion of the target pedestal. A vertical motion through a distance V as indicated translates the plane of the target ladder rods from R_1 to R_3. Determination of the angles β and δ is discussed in the text.

$$p = (p_o + \beta V) \cos (\theta_T - \theta_o) + \delta(\theta_o)V \quad (15)$$

yields p_o, β, δ, and their standard deviations. The results are given in Table VI.

The misalignments and uncertainties represented by p_o, β, and δ affect the determination of the scattering geometry by way of η, x_p, z_p and x'_p. Aside from finite target thickness effects, η is determined entirely by p; that is

$$\eta = p_o + \beta V + \eta', \quad (16)$$

where η' is measured from the target plane. We retain p_o in eq (16) even though its value is zero, for purposes of error propagation. The effects of imperfect target pedestal alignment ($p \neq 0$) on the scattering angle and solid angle are always very small, less than 10^{-2} degrees and 3 parts in 10^4, respectively, for V up to ten inches.

Since the targets oscillate horizontally, the measurements described above were checked while the target was oscillated. Changes in dial gauge readings were less than 0.2×10^{-4} inches from the average value, and the effect is negligible.

Horizontal target motion was calibrated with a dial gauge whose plunger is aligned with the oscillation direction. The total travel is 0.461 inches. Through the central 0.3 inches of this range, the motion is a linear function of the number of pulses provided by the stepping motor drive. The average slope is $\Delta = (2.83 \pm 0.03) \times 10^{-3}$ inches/step, and is not measurably different for the two directions of motion. Individual position measurements scatter about the best fit straight line with a standard deviation of about 0.5×10^{-3} inches.

The next step in the target assembly alignment is to measure the location of the assembly relative to the spectrometer. The procedure is described in section II and the results presented in figure 10 and Table I. By definition, the axis of rotation of the target pedestal passed through the origin when the calibration was performed, except for the effect of $\delta(\theta_o)V$ in eq (15). In section II, we discussed the lack of rigidity of the target support assembly, and the necessity of returning the assembly to its original position, represented by the values of D-B and A-C in Table I. In practice it is difficult to return the pedestal to exactly the desired point. Instead, we correct the values of x_p, z_p, and z'_p for the differences between the pedestal dial gauge readings and their original values. Since the indicator ring is 9 1/4 inches below nominal beam height, and the motion involved is not a pure translation of the pedestal, we measured the tilting motion that accompanies horizontal motion by autocollimation techniques employing a mirror mounted in the target ladder. These measurements show that the target axis at beam height moves $S_v = 1.156 \pm .005$ times as far as the indicator ring for all small horizontal motions, independently of the direction of motion. Combining this effect with the effect represented by eq (15), we obtain

$$x_p = V[\cos\theta_o \delta(270°) - \sin\theta_o \delta(180°)] - (S_v/2)\,[(A - C) - (A - C)_F], \qquad (17)$$

$$z_p = -V[\sin\theta_o \delta(270°) + \cos\theta_o \delta(180°)] + (S_v/2)\,[(D - B) - (D - B)_F], \qquad (18)$$

and

$$x'_p = V\,\delta(270°) - (S_v/2)\Big\{[(A - C) - (A - C)_F]\cos\theta_o + [(D - B) - (D - B)_F]\sin\theta_o\Big\}, \qquad (19)$$

where (D - B) and (A - C) are the differences in readings of the appropriate dial gauge pairs. The unsubscripted values refer to any given experimental setup, and the values with subscript F are the fiducial values listed in Table I.

In addition to the translational motion, twisting of the target pedestal is also observed. The main source of twisting is a torque accidentally applied to the scattering chamber when it is connected to the spectrometer flange. Reasonable care in making this connection will cause errors estimated to be less than 10^{-2} degrees in target angle, less than 2 parts in 10^4 in solid angle, and no effect on the scattering angle.

V. Realization of the Baseline

The baseline is defined to be the horizontal line through the origin point 0 and the center of the quadrupole exit flange, P, as shown in figure 19. A theodolite placed on this line is used to locate the axes of the upstream beam scanners and the spectrometer horizontal aperture slit center relative to the baseline. The aperture center is located only for a reference spectrometer angle, $\theta_o \simeq 180°$. Subsequently, all other values of θ_o are calibrated relative to the reference angle.

A reference point at the origin (i.e., on the axis of rotation) is realized by a

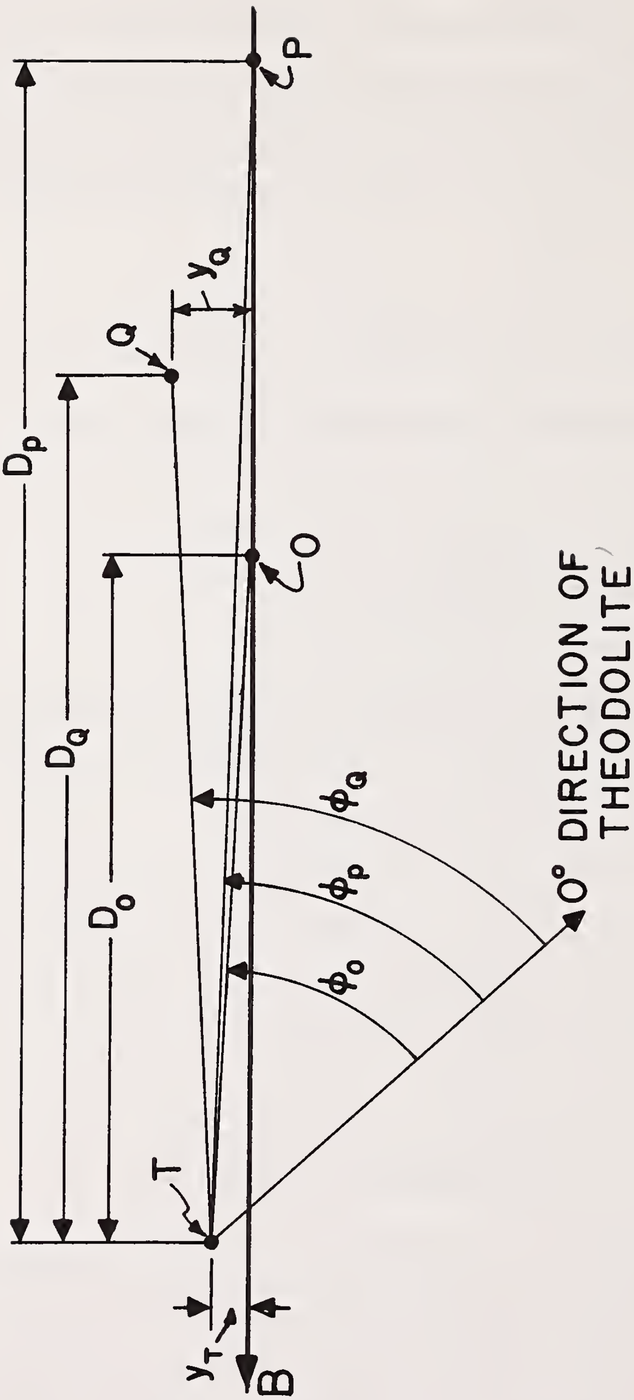

Figure 19. Method of surveying the baseline with a theodolite located at T. The points O and P define the baseline, and Q represents any other object to be located relative to the baseline which is indicated by the line labelled "B".

fixture in the shape of a right circular cylinder surmounted by a cone, machined so that the apex of the cone is accurately on the axis of the cylinder, with the axis perpendicular to the base of the cone. The fixture is placed on the target turntable, near its center, with the ladder rods removed and the horizontal oscillation cam disengaged. A dial gauge is mounted to the support assembly, with its plunger contacting the cylindrical surface of the fixture. The turntable is rotated and variations in the dial gauge readings noted. The position of the fixture on the turntable is adjusted until the dial gauge reading is invariant under rotation. The fixture and thus the cone apex is then accurately on the axis of rotation. A second dial gauge, mounted at right angles to the first, is used simultaneously for improved speed and accuracy. The fixture can be centered well enough so that neither dial gauge deviates from its average reading by more than 2×10^{-4} inches during a full 360° rotation. When properly positioned, the cone apex appears to be stationary when it is sighted from the theodolite 18 feet away and the target pedestal is rotated.

The sighting marker at the quadrupole exit flange is a tightly fitting lucite disk, embedded with fine wire cross hairs passing through its center. When the disk is rotated in the flange, or removed and repositioned, no motion of the cross hair center can be seen from the theodolite.

The theodolite is placed within .02 inches of the baseline, and its position measured by triangulation, as indicated in figure 19. Distances along the baseline are measured with a steel tape ruler to an accuracy of 0.1 inch, resulting in essentially no error in locating the components relative to the baseline. A set of measurements of angles (ϕ_O, ϕ_P, ϕ_Q) and distances (D_O, D_P, D_Q) as indicated in figure 19 yield the transverse offset, y_Q, of any component, Q. Since the angular difference between any pair of theodolite settings is typically 10 arc seconds for these measurements, the limiting factor in locating the components along the baseline is the visibility of the components and reference markers rather than the quality of the instrument. Systematic effects are reduced by illuminating all viewed objects symmetrically and approaching the sight line from opposite directions. The standard deviation of individual angle measurements is about 2 arc seconds (10^{-5} radians).

The 180° reference position of the spectrometer is established as indicated above.

The displacement, y_Q, of the center of the horizontal aperture slits, with the slits closed to the limit positions, is determined by the method described. The distance, L_X, from the origin 0 to the aperture slit center, together with y_Q, determine the offset of the spectrometer angle from 180°. In addition to L_X and y_Q, the spectrometer angle is a function of the radial dial gauge reading, $\mathcal{R}$, the azimuthal dial gauge reading, $\mathcal{D}$, and of D-B and A-C. The corrections for $\mathcal{R}$, $\mathcal{D}$, and the target pedestal dial gauges are discussed in section VI. It should be noted that the correction for the target pedestal dial gauges is different from the one described by eq (17) - (19). That correction accounts for motion of the target pedestal; the correction needed here is for the undesired motions in the spectrometer support assembly to be discussed in section VI. During the measurement process described here the target pedestal was not disturbed.

The 180° reference position was measured independently three times. Averaging the three sets of data gives the fiducial angle $\theta_F(180)$, and an estimate of the measurement error, which are given in Table II.

The center of rotation of the upstream horizontal beam scanner, x_C, is also measured relative to the baseline by triangulation. The theodolite is sighted on the lucite rod of the scanner, with the rod near its center of travel, i.e. $x_R \simeq 0$, by setting $N \simeq N_o$. A second sighting is made after rotating the scanner by exactly 100 steps. Since the average of these two values of x_R is zero, the average of the two sighting directions passes through the center of rotation.

Vertical measurements are made in a manner similar to the horizontal ones, except that only one fixed point is needed since the baseline is defined to be horizontal in space. The leveling bubble of the theodolite determines the horizontal direction. Forward and reverse transit readings are taken in order to minimize theodolite errors. The heights measured are the standard Bullseye center, the center of the vertical aperture slits, and the axis of rotation of the upstream vertical beam scanner. Defining the bullseye height as y = 0, the latter two heights are y_A and y_C, respectively.

Table II summarizes the results of all measurements described in this section. Errors listed for θ_F, x_C, y_A, and y_C are standard deviations of the means, based on the variance of the individual measurements. Values of B_X and B_y, which are defined under eq (8) and (9), respectively, are also given in the table.

VI. Scattering Angle

Having established the fiducial angle $\theta_F(180)$, all other spectrometer angles can be measured relative to $\theta_F(180)$ by means of a theodolite located on the axis of rotation. For each nominal scattering angle, a theodolite measurement of the angular difference from $\theta_F(180)$ is made. In all cases the object sighted is the center of the horizontal aperture slits, with the slits set at their limit positions. With each angle measurement, a set of dial gauge readings is taken, since the spectrometer angle is strongly correlated with the azimuthal gauge reading, $\mathcal{D}$, and weakly correlated with the radial reading, $\mathcal{R}$. Auxiliary measurements made by changing $\mathcal{D}$ and $\mathcal{R}$ establish these dependences. All spectrometer angle measurements can thus be reduced to a set of fiducial angles θ_F corresponding to arbitrary fiducial values of $\mathcal{D}$ and $\mathcal{R}$.

In the course of these measurements, "random" motions of the spectrometer relative to a fixed coordinate system were discovered. The target pedestal dial gauge readings were found to be correlated with the random motions, and were used to perform some corrections to the θ_F calibrations. The errors in this correction procedure can be estimated with sufficient accuracy to establish that the calibration concept is valid. Thus, θ_o can be obtained from a set of measured quantities to the desired accuracy of $< 0.01°$, without having to resurvey the apparatus each time the scattering angle is changed.

A. Theodolite Alignment

In order to use a theodolite to measure the scattering angles, it is essential to locate the theodolite at the chosen origin, that is, on the axis of rotation. Since the sighting distance is only about 24 inches, the accuracy required is about 5×10^{-4} inches to limit the angular error to 10^{-3} degrees. This accuracy was achieved with the use of auxiliary dial gauges by the method illustrated in figure 20. The theodolite is set up as close as possible to the axis of rotation of the target pedestal and sighted on a convenient marker (some 15 ft. distant). Two dial gauges are mounted from the target pedestal baseplate with their plungers contacting the body of the theodolite. Next the target pedestal is rotated through approximately 90°, while the theodolite is rotated through exactly the same angle in the opposite direction by continuing to sight the original

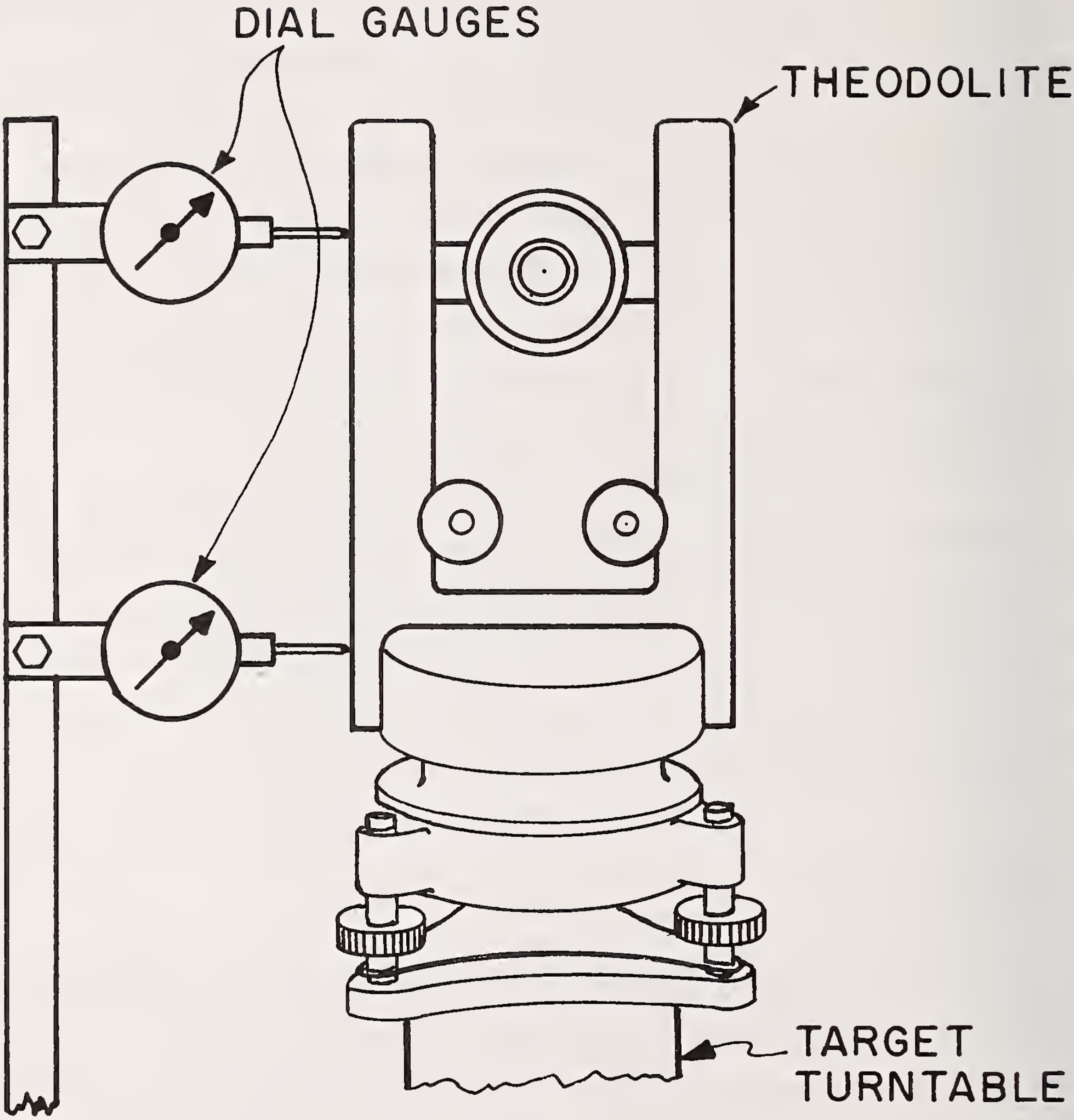

Figure 20. Setup for aligning the theodolite on the axis of rotation.

marker. Any changes in dial gauge readings are noted. The procedure is repeated until a full rotation has been made. Both dial gauge readings will remain constant under this procedure _if and only if_ the axes of rotation of the target pedestal and of the theodolite coincide. In addition to the usual leveling screws for tilt adjustment, the theodolite is equipped with a screw-operated translation stage so that it can be adjusted in successive approximations until the coincidence of axes is obtained. After final adjustment, the dial gauge at the elevation of the theodolite eyepiece (i.e., nominal beam height) does not deviate more than 1.5×10^{-4} inches from its average reading at any point in the rotation. The attendant residual error in scattering angle is less than 4×10^{-4} degrees. The second dial gauge, located about 5 inches below nominal beam height deviates by no more than 7×10^{-4} inches from its mean reading. Thus the axis of rotation and the theodolite vertical axis are parallel to within 1.4×10^{-4} radians and the resulting error in scattering angle is negligible since all sightings are made in the horizontal plane.

If the optic axis of the theodolite does not pass through its axis of rotation, no error in scattering angle would result, provided that the sighting distance remained constant as the spectrometer is rotated. However, the pivot-to-slit distance, L_x, does change slightly with angle. Since the maximum variation in L_x is less than 0.05 inches, the angular error due to the location of the optic axis is less than 8×10^{-5} radians per inch offset. The offset in the instrument is thought to be less than 0.001 inches, but in order to use the theodolite at 24-inch sighting distance, we added a close-up lens in front of the theodolite objective, which could shift the optic axis. By sighting the same object with and without the close-up lens (this is possible at one sighting distance -- about six feet), we measured the offset to be certainly less than 0.05 inches, which gives a negligible error in the scattering angle.

The physical height of the theodolite required that the target pedestal be lowered by 4 3/8 inches from the reference target position to place the theodolite eyepiece at nominal beam height. Because of the misalignment of the axis of rotation relative to the direction of vertical pedestal motion discussed in section IV, the theodolite was not at the defined origin point 0, but at a point analogous to P in figure 14. For each value of θ_o measured with the theodolite we must correct the observation for this offset. Using eq (17) and (18), with the terms dependent on A, B, C, and D set to zero, the correction is

$$\theta_{measured} - \theta_o = \frac{x_p}{L_x - z_p} .$$

Since the z_p term has a completely negligible effect, we apply the correction in the form

$$\theta_o = \theta_{measured} - \frac{V}{L_x} [\cos \theta_o \; \delta(270) - \sin \theta_o \; \delta(180)] . \qquad (20)$$

This correction, which has been applied in obtaining the values of θ_F listed in Table I, never exceeds 5×10^{-3} degrees. The error in this correction due to uncertainties in $\delta(270)$ and $\delta(180)$ is a systematic function of angle. The error in the angular difference between θ_o and the reference angle (180°) is

$$E(\theta_o - 180°) = \frac{V}{L_x} [(1 + \cos \theta_o)^2 \; \varepsilon^2(270) + \sin^2 \theta_o \; \varepsilon^2(180)]^{1/2} , \qquad (21)$$

where $\varepsilon(\theta)$ is the error in $\delta(\theta)$.

The reproducibility of the angle measurements is deduced by comparing sets of angle readings taken without moving the spectrometer. Averaging over all such sets of data, the standard deviation of a single measurement is about 2 arcseconds (6×10^{-4} degrees). This reproducibility takes account of theodolite motion between readings, our ability to center the theodolite sighting at the slit center, and the readability of the theodolite scales (the least count is one arcsecond).

B. Azimuthal Dial Gauge Calibration

The azimuthal dial gauge measures the difference between the spectrometer angle θ_o and a fiducial angle θ_F. Our definition of θ_F includes the requirement that the azimuthal gauge reading is $\mathcal{D}_F$ = 0.5000 inches, except at $\theta_F(180)$ where $\mathcal{D}_F$ = 0.4902 inches. To determine the dependence of θ_o on $\mathcal{D}$, we set $\mathcal{D}$ to 0.9000 inches and to 0.1000 inches by rotating the spectrometer and measuring the angular motion of the spectrometer aperture slits with the theodolite mounted at the axis of rotation. The result for the average of two independent determinations is

$$\frac{\Delta\theta}{\Delta\mathcal{D}} = -1.2566 \pm 0.0004 \text{ degrees/inch} , \qquad (22)$$

from which we can compute θ_o from θ_F with an error in θ_o due to the uncertainty in $\frac{\Delta\theta}{\Delta\mathcal{D}}$ plus higher order geometrical effects (see figure 15 for the actual geometry) of less than 2.5×10^{-4} degrees for any value of $\mathcal{D}$ between 0.0 and 1.0 inch.

C. Radial Dial Gauge Correction

In connecting the spectrometer vacuum chamber to a scattering port, the spectrometer is moved radially so that the target pedestal dial gauges remain at their correct readings; thus, the radial position of the spectrometer is not a free variable. In fact, when the spectrometer angle calibration was made we did not know the required radial position to better than $\pm$ 0.03 inches. Because transverse motion accompanies radial motion we need to know the change in θ_o caused by changing the radial position, as measured by R, in order to compute θ_o. The calibration is made by measuring the change in the angle to the aperture slits, as seen by the theodolite at the axis of rotation, as the spectrometer is moved radially inward (i.e., increasing R). The direction is specified because there appears to be a small hysteresis between inward and outward travel. In connecting the vacuum system, the spectrometer is normally moved inward to its final position. A set of such measurements taken with the spectrometer near the 180° position gave $\Delta\theta/\Delta R = 0.0472 \pm 0.0002 \frac{\text{degrees}}{\text{inch}}$, for $0.3 < R < 0.8$ inches. No deviation from linearity was observable in this data set. The dependence of $\Delta\theta/\Delta R$ on spectrometer position was checked at a nominal scattering angle of 93° with the result that $\Delta\theta/\Delta R = 0.035 \pm 0.003$ degrees/inch, in poor agreement with the 180° result. Due to an error in data reduction, this discrepancy was not noticed in time to study the effect further. We therefore adopt the careful measurement as our best value of the effect, ignore any dependence on spectrometer angle, and adopt the difference between the two values as a measure of the error:

$$\frac{\Delta\theta}{\Delta R} = (0.047 \pm 0.012)\ \frac{\text{degrees}}{\text{inch}}\ , \qquad (23)$$

which is the solid line in figure 3. Fiducial angles are defined to be the values of θ_o that occur when $R_F = 0.700$ inches and $\mathcal{D}$ is at its fiducial value, $\mathcal{D}_F$. The spectrometer angle measurements were made with R between 0.689 and 0.700 inches; thus, the largest correction applied for the $\Delta\theta/\Delta R$ effect was $(5.2 \pm 1.3) \times 10^{-4}$ degrees. Subsequently, we have found that the spectrometer always connects to the scattering chamber with R in the range 0.67 to 0.73 inches. Thus, the radial correction never exceeds $\pm$ 1.4 x 10^{-3} degrees, and the uncertainty in scattering angle due to the estimated error in $\Delta\theta/\Delta R$ never exceeds $\pm$ 4 x 10^{-4} degrees.

D. Fiducial Angle Measurements

The chronology of the fiducial scattering angle calibration was:

1. The baseline was surveyed.
2. The spectrometer was moved to $\theta_F(180)$ and surveyed relative to the baseline.
3. The theodolite was aligned on the axis of rotation.
4. The theodolite angle to the horizontal aperture slits was measured.
5. The spectrometer was rotated successively to the other nominal angles, 168°, 145° ..... 58°, 40°, and the theodolite angle to the aperture slits measured at least twice at each angle.
6. The spectrometer was moved to about 38°, then back to 40°.
7. The theodolite angle to the slits was remeasured at 40°, and successively at the other nominal angles, ending with a second measurement at $\theta_F(180)$.
8. The theodolite was removed from the target pedestal and placed on the baseline.
9. The baseline was resurveyed including the aperture slit location needed to determine $\theta_F(180)$.

The two full sets of measurements of angular differences between each fiducial angle and $\theta_F(180)$, were found to be systematically disparate, indicating a correlation with the direction of rotation of the spectrometer. With each theodolite angle measurement we have a full set of dial gauge readings. Most of the data was taken with $\mathcal{D}$ = 0.5000 inches, although a few points were taken at other values to calibrate the azimuthal dial gauge. The radial spectrometer position was not adjusted, but the radial gauge reading, R, was recorded each time. A range of variation of 0.011 inches was observed, presumably due to slight non-rigidity of the spectrometer support system coupled, perhaps, with the main bearing not being absolutely horizontal. (The bearing could be out of horizontal by 5 x 10^{-4} radians. Since the total weight is about 5 x 10^{4} kg, there could be a 25 kg force in the plane of the bearing.) Fortunately, we also recorded the target pedestal dial gauge readings (A, B, C, D) with each angle measurement, which helped greatly in understanding the systematic differences in the measurements.

E. Target Pedestal Dial Gauge Effect

A systematic difference, averaging 3.2×10^{-3} degrees, was detected between the angle measurements made while rotating the spectrometer toward smaller scattering angle and those made while rotating in the reverse direction. The anticipated sources of errors, which have been discussed above, are too small to explain the observed effect. (The corrections which are systematic functions of scattering angle have no effect, of course.) The angular differences between forward and reverse measurements are strongly correlated with differences in D-B values taken at the same time, as shown in figure 21. The variation in spectrometer angle with D-B reading is

$$\frac{\partial\theta}{\partial(D-B)} = 2.52 \pm 0.44 \text{ degrees/inch.} \qquad (24)$$

The quoted error is the standard deviation obtained from a least squares fit to the data points. There is no statistically significant variation of θ with (A-C). If we assume

$$\delta\theta = \frac{\partial\theta}{\partial(A-C)}\,\delta(A-C) + \frac{\partial\theta}{\partial(D-B)}\,\delta(D-B)\ ,$$

we find $\frac{\partial\theta}{\partial(A-C)} = 1.5 \pm 2.2$ and $\frac{\partial\theta}{\partial(D-B)} = 2.8 \pm 0.6$ degrees per inch, but the quality of fit is somewhat poorer than for the case where a dependence on D-B only is assumed. We therefore adopt the simpler hypothesis that the deviation is a function of D-B only.

It is easy to show that the observed effect is not due to real motion of the target pedestal alone. If the target pedestal moved, the change in scattering angle could be computed from the dial gauge reading changes, knowing the target-to-aperture distance. This effect would be $\frac{\partial\theta}{\partial(A-C)} = -1.2$ degrees per inch, $\frac{\partial\theta}{\partial(D-B)} = 0$ (to first order), in disagreement with the observed variation.

We conclude that the spectrometer angle is not a unique function of $\mathcal{D}$ and R as expected. The main spectrometer bearing could have a looseness which permits motion of the rotating part of the bearing relative to the stationary part. If (A-C) and $\mathcal{D}$ are constant, this is a rotation about the point of contact of the $\mathcal{D}$ dial gauge. However, if this were a rigid

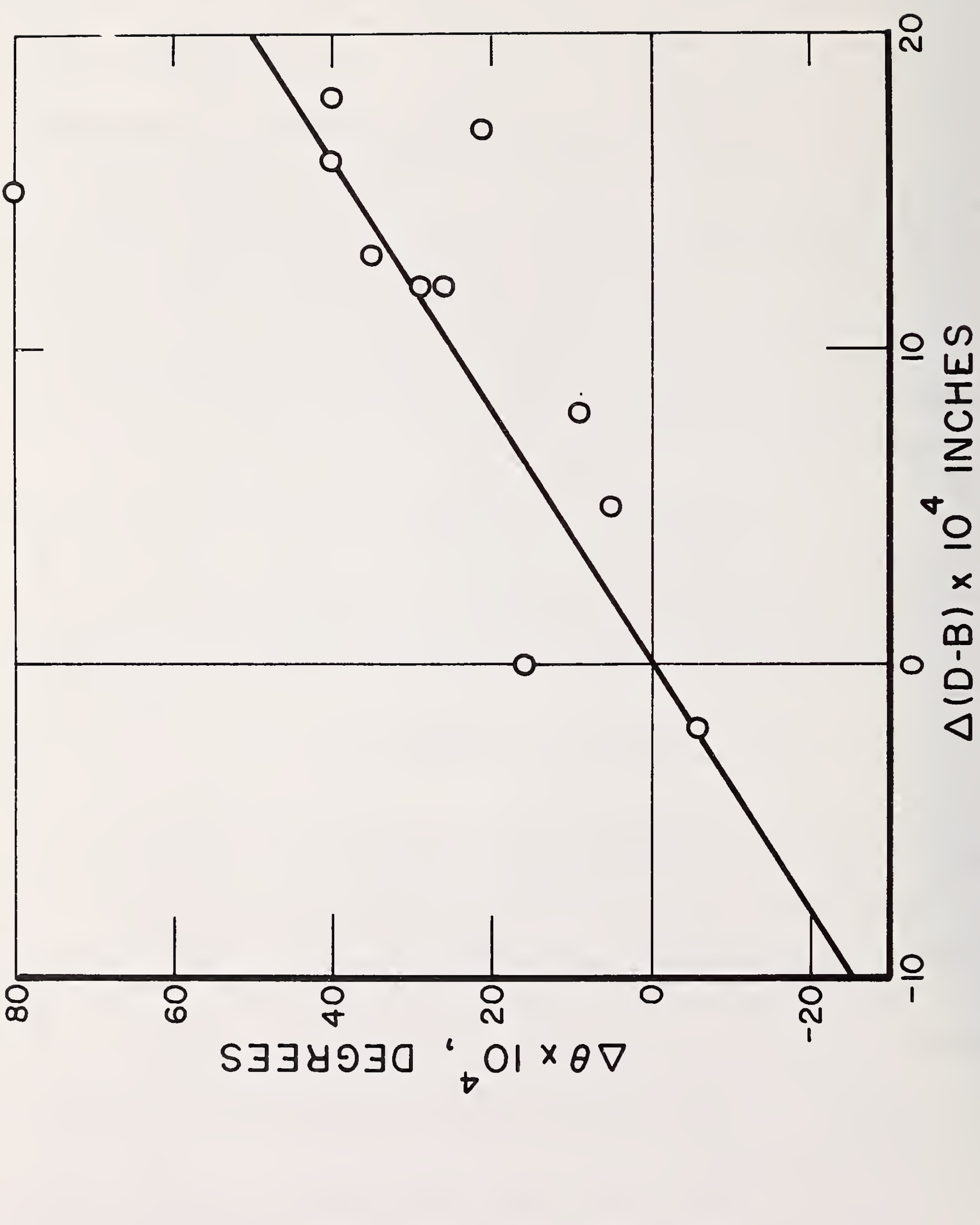

Figure 21. Differences of pairs of scattering angle measurements plotted against the difference of the corresponding (D-B) measurements. The solid line is the best fit to the data $\frac{\partial\theta}{\partial(D-B)} = 2.52 \pm 0.44$ degrees per inch.

body rotation, the effect on the sighting angle to the slits would be only 0.6 degrees per inch change in (D-B).

To handle this problem, a variation of the actual scattering angle which correlates with D-B according to eq (24) is assumed and the calibration data is corrected for this effect. Once the calibration was completed, real motion of the target pedestal was permitted and we can no longer distinguish between real pedestal motion and the apparent motion. Therefore, each time a new scattering angle is set up there is an uncertainty in the target location equal to the standard deviation of the target pedestal dial gauge readings observed during calibration and an uncertainty in scattering angle, measured from the defined origin, 0, equal to the variation in the pedestal gauge readings multiplied by the correlation factor of 2.52 degrees/inch. During the calibration, five independent sets of pedestal dial gauge readings were taken: two with scattering angle data, two with the solid angle data, and one with the target angle data. The average values of (D-B) and (A-C) are listed in Table I and plotted in figure 10. The standard deviation of the mean at each nominal angle is 1.1×10^{-3} inches, and the standard deviation of a single value is 2.2×10^{-3} inches. Thus, there is an uncertainty of 1.1×10^{-3} inches each in target coordinates x_T and z_T. There is an additional uncertainty in scattering angle, θ_o, of (2.52 deg./in) x (2.2×10^{-3} in) = 5.5×10^{-3} degrees. Since x_T is in the direction measured by (A-C) and only (D-B) motion changes θ_o, these two uncertainties can be treated as independent. The uncertainty in θ_o is correlated with the change in solid angle due to change in target-to-aperture distance. The solid angle effect, 1 part in 10^4, is much smaller than the θ_o effect of 3 to 6 parts in 10^4 on the calculated cross section.

F. Fiducial Angle Results

The angles, θ_m, measured by the theodolite at the axis of rotation are converted to fiducial angles, θ_F, by combining the corrections expressed by eq (20), and (22) through (24) to obtain

$$\theta_F = \theta_m - \frac{V}{L_x}[\cos\theta_o\,\delta(270) - \sin\theta_o\,\delta(180)] + 1.2566\,(\mathcal{D}-\mathcal{D}_F)$$

$$- 0.047\,(\mathcal{R}-\mathcal{R}_F) - 2.52\,[(D\text{-}B) - (D\text{-}B)_F] + G\,, \qquad (25)$$

where the constant G is needed because the theodolite has an arbitrary zero angle direction. G is obtained from the 180° measurements, since in that case $\theta_F(180)$ is known from the base line calibration. Unsubscripted variables $\mathcal{D}$, R, (D-B), are observed values. The corresponding variables with subscript F are the fiducial values.

The values of θ_F given in Table I are the averages of two determinations, except at 180° and 145° where three determinations are used. The standard deviation of a single measurement is 1.5×10^{-3} degrees. Therefore, the random error associated with each θ_F is 1.0×10^{-3} degrees. The random error in $\theta_F(180)$ of 3.3×10^{-3} degrees is a common error for all other fiducial angles since this error is associated with the term G in eq (25). The sources of error in θ_F are summarized in Table III.

G. Scattering Angle Equation

The scattering angle, θ_o, is calculated from

$$\theta_o = \theta_F + \frac{\Delta\theta}{\theta\mathcal{D}} (\mathcal{D} - \mathcal{D}_F) + \frac{\Delta\theta}{\Delta R} (R - R_F)$$

$$= \theta_F - 1.2566(\mathcal{D} - 0.5000) + 0.047(R - 0.7) \ . \qquad (26)$$

The values of θ_F are given in Table I, and $\mathcal{D}$ and R are dial gauge readings in inches. There are no terms in eq (26) involving the target pedestal gauges or the pedestal axis misalignment because of the definition of θ_o we have chosen. These sources of error affect only the target location (x_T, z_T). The total error in scattering angle includes uncertainties in the terms of eq (26) as well as uncertainties in the target location and beam direction. The largest sources of error are the uncertainty in the fiducial angles, $\leq 4.1 \times 10^{-3}$ degrees, and the target pedestal dial gauge effect, 5.5×10^{-3} degrees. However, the uncertainty in (D-B) also affects the scattering angle through α_x, and the solid angle through z_T. Similarly, other sources of error (e.g., (A-C), $\delta(270)$, $\delta(180)$, etc.) enter into the total cross section uncertainty by several routes.

VII. Solid Angle

The acceptance solid angle of the spectrometer is defined by the aperture slits. In this section we describe the measurements which determine the distances L_x and L_y and the angles γ_x and γ_y. All other quantities entering into the determination of solid angle have already been discussed, i.e., the target coordinates (x_T, y_T, z_T), the aperture openings H and W, and the slit edge radii R_S.

The difference between L_y and L_x is measured with a micrometer depth gauge as illustrated in figure 22. A ground flat steel plate is placed against the horizontal aperture defining cylinders and a depth gauge is placed in contact with the vertical aperture defining cylinders. Since all cylinders have equal diameters, the desired distance is simply the depth gauge reading plus the plate thickness,

$$\Delta L = L_x - L_y = 2.648 \pm 0.001 \text{ in.} \tag{27}$$

Figure 23 illustrates the method by which L_y was measured. A precision ground steel sphere, 1.0 inch in diameter, is located on the axis of rotation of the target pedestal employing the technique described in section V for centering the conical marker. A measuring rod of length L_R, consisting of an aluminum rod capped with a second precision ground steel sphere, is positioned with the spherical end contacting the vertical aperture cylinders. The spectrometer is moved radially inward until the end of the measuring rod contacts the first sphere. The reading, R, of the radial dial gauge is noted at the point of contact. A simple geometry calculation yields the result

$$L_y(R) = L_R + r_2 - r_1 + \sqrt{2R_s r_1 + r_1^2 - HR_s - H^2/4} \; . \tag{28}$$

Equation (28) is valid only if the rod is held horizontal, with its spherical end centered left to right along the aperture-defining cylinders. The rod was held horizontal to within 1/16 inch and centered to within 1/8 inch, thus causing an error in L_y of less than 5×10^{-4} inches. The rod length, measured at thermal equilibrium in a temperature controlled room, was L_R=19.9955 ± 0.0002 inches at 73°F. The temperature in the spectrometer room was 5.8° lower when the calibration was made, requiring a correction of -0.0014 inches for thermal contraction of the aluminum rod (12.4×10^{-6} °F^{-1}). Both steel spheres have radii 0.5000 ± 0.0002 inches, and the one at the axis of rotation was centered to within $\pm 2 \times 10^{-4}$ inches. The aperture cylinders have R_S = 0.8750 ± 0.0005. The aperture H, measured for the present purpose with a feeler gauge, was 0.0302 ± 0.0005 inches. The fringe counter system (see section II) was checked during the calibration to be sure that the aperture was not changed by the pressure of the measuring rod against the slits,

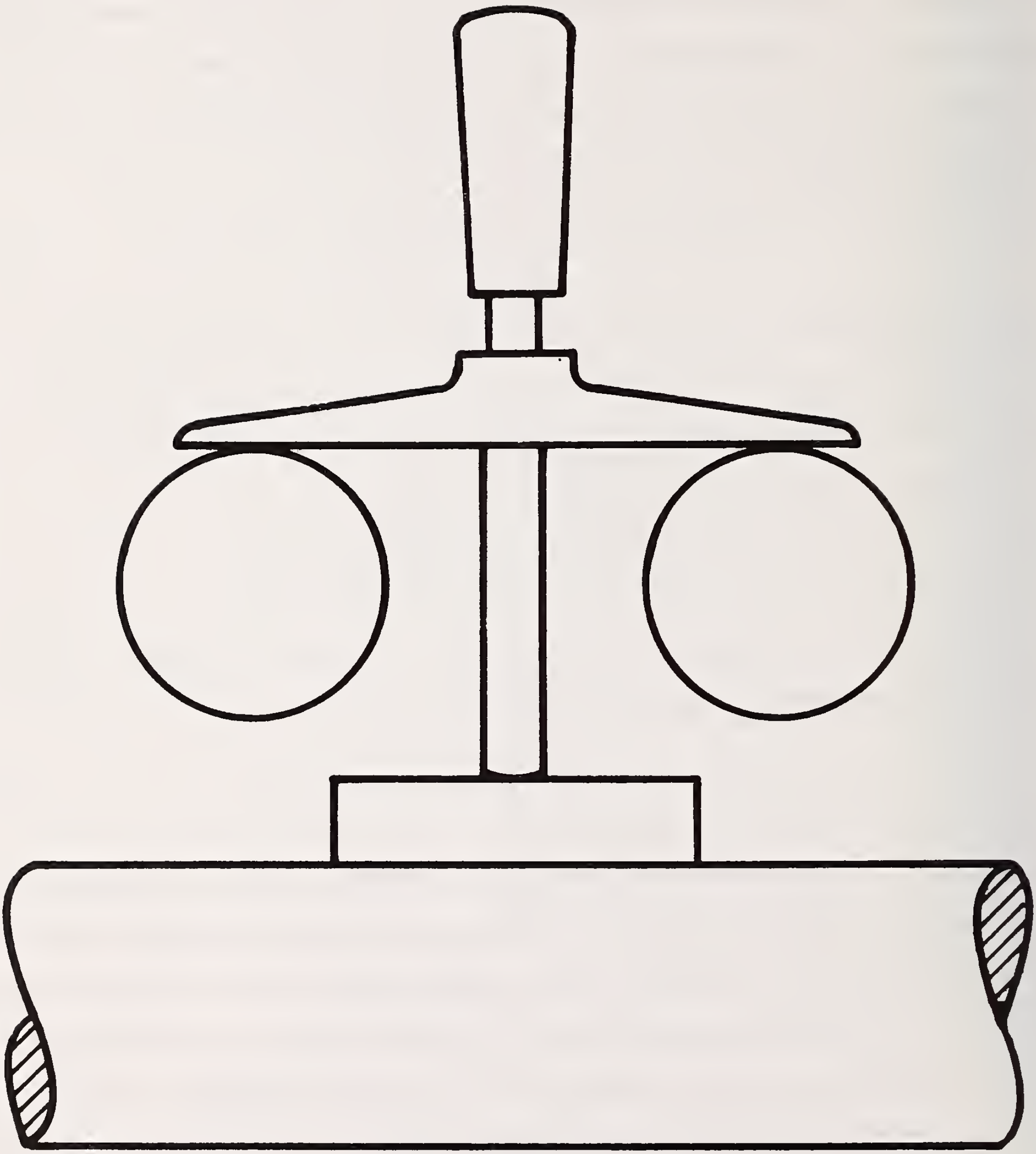

Figure 22. Method for measuring $L_x - L_y$.

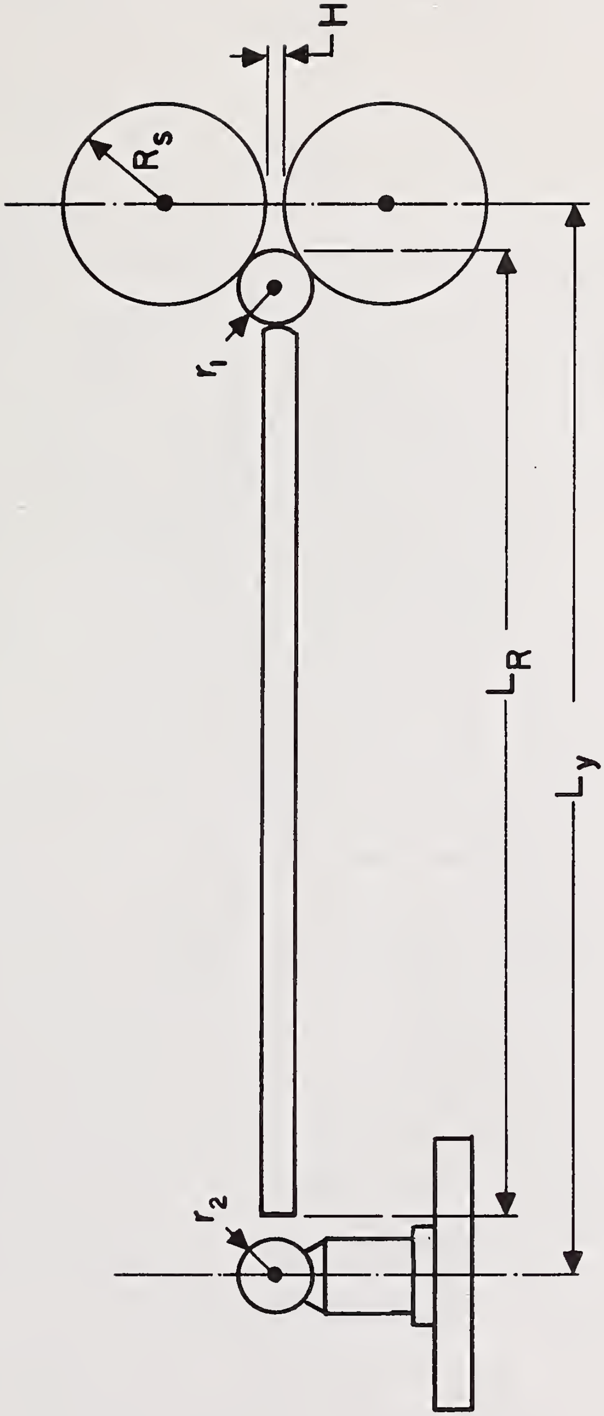

Figure 23. Setup for measuring L_y, side view.

and a change of 1×10^{-4} inches was noted. These uncertainties are propagated through eq (28) and combined in quadrature to obtain an uncertainty of 7×10^{-4} inches which we take to be the systematic error in L_y.

To obtain the origin-to-slit distance as a function of the radial position of the spectrometer, a calibration of the form

$$L_y = L_o(\theta_F) + \left(\frac{\partial L_y}{\partial \mathcal{R}}\right)(\mathcal{R} - R_F) \tag{29}$$

is needed, where R_F is chosen to be the same value as for the θ_o calibration. The fiducial length L_o is a function of angle because the spectrometer does not execute a pure rotation about the origin. The slope, $\partial L_y/\partial \mathcal{R}$, is expected to be -1.0 because the radial dial gauge sensing direction is parallel to the radial spectrometer motion and the gauge reading increases as the spectrometer moves forward. Because of the imperfections in the spectrometer motion, we measured the slope at each nominal scattering angle, by adding caps to the measuring rod which increases its length by about 0.1 and 0.2 inches. The slope varied from -0.998 (at 163°) to -1.006 (at 110°) with an average value of -1.0027. The validity of this value is questionable since the average value would be exactly -1.0 if there were an error of 5×10^{-4} inches in the thickness of the 0.2 inch cap. We therefore adopt the value of $\partial L_y/\partial \mathcal{R} = -1.0$ and assume conservatively that its accuracy is better than $\pm 6 \times 10^{-3}$, corresponding to the largest observed deviation. In the final calibration, with no caps on the measuring rod, the values of $\mathcal{R}$ at the contact point were between 0.716 and 0.752 inches. The error in L_o due to the uncertainty in the slope is thus always less than 3×10^{-4} inches. The calibration consisted of measuring the value of $\mathcal{R}$ at which contact is made with the spectrometer at each fiducial angle ($\mathcal{D}_F$ = 0.500 in.). Two values were obtained at each angle, one while rotating forward (163° → 40°), and again during the reverse rotation. For each measurement we obtain a value of $L_o(\theta_F)$ from eq (29), along with target pedestal dial gauge readings (D-B) and (A-C). A correlation between changes in L_o and changes in D-B was observed, given by

$$\frac{\partial L_o}{\partial(D-B)} = -0.94 \pm 0.30 \tag{30}$$

A rigid-body motion of the entire rotatable structure would give $\partial L_o/\partial(D-B) = -1/2$. As expected, there is no significant dependence on (A-C). Here, as in the case of the scattering angle, we conclude that some non-rigid motion can occur during rotation of the spectrometer, but we can correct the calibration data for its effect. Thus, for each measured $\mathcal{R}$,

$$L_o(\theta_F) = L_y + (\mathcal{R} - 0.700) - 0.94\,[(D\text{-}B) - (D\text{-}B)_F]\ , \qquad (31)$$

with L_y obtained from eq (28). The two values of L_o for each θ_F are averaged to obtain the values listed in Table I. From the variance of the individual measurements, the random error of each L_o value in Table I is 5×10^{-4} inches. The largest correction made for the last term in eq (31) was 0.0024 inches, with a corresponding uncertainty of 8×10^{-4} inches. The errors in the L_o determination are summarized in Table IV.

To calculate L_y and L_x for a given experimental setup, eq (27) and (29) are used with $\partial L_y/\partial R = -1.0$ and $L_o(\theta_F)$ taken from Table I. No correction is to be made for the pedestal dial gauge effect, for the same reasons given at the end of section VI. The uncertainty in each L_y and L_x value due to this effect is 2.1×10^{-3} inches, which is obtained from eq (30) and the 2.2×10^{-3} inch standard deviation of D-B. Note that no correction is made for the azimuthal dial gauge, i.e., for $\theta_o \neq \theta_F$. This is valid since $L_o(\theta_F)$ changes at most by 9×10^{-3} inches between adjacent fiducial angles, whereas $|\theta_o - \theta_F| \leq 0.6$ degrees. Thus we expect the θ_o dependence of L_y to be less than 3×10^{-4} inches.

The aperture slit system is bolted to the entrance flange of the spectrometer vacuum chamber. This flange is not precisely perpendicular to the optic axis of the spectrometer. The solid angle depends (weakly) on the angle between the normal to the plane of the aperture slits and the Z axis. Optical autocollimation is used to measure this angle. The theodolite is mounted on the baseline, as described in section V, some 18 feet upstream of the target location, and sighted on the axis of rotation. A front-surfaced plane mirror, mounted in a target holder so that its reflecting surface is in the target plane (vertical within 4×10^{-4} radians), is rotated until the theodolite is sighted on the center of the aperture slits. Next, a second front-surface mirror made from an optical flat is held flat against the aperture slits. If the plane of the aperture were perpendicular to the Z axis, one would then see the objective lens of the theodolite centered in the field of view. The displacements, horizontally and vertically, of the theodolite in the field of view measure γ_x and γ_y, respectively. The method is not highly accurate (the standard deviation is about 0.5×10^{-3} radians), but is sufficient since the solid angle is very weakly dependent on γ_x and γ_y. The same result occurs whether the mirror is held against the horizontal slits or the vertical slits, confirming the parallelism of the planes of the two pairs of slits. Measurements with the spectrometer at $\theta_o = 40°$ and 93° give the same result for γ_x within 1×10^{-3} radians, and for γ_y within 2×10^{-3} radians. The differences with scattering angle are presumably due to the spectrometer symmetry plane not pointing precisely toward the axis of rotation and the axis of rotation of the spectrometer not being exactly vertical. The variations of γ_x and γ_y with scattering angle are negligible, so we adopt the average value of the measurements taken as being applicable to all scattering angles. The result is

$$\gamma_x = (5 \pm 1) \times 10^{-3} \text{ radians},$$

and (32)

$$\gamma_y = (-5 \pm 1) \times 10^{-3} \text{ radians}$$

The effect of γ_x and γ_y on the cross section would be negligible if the target were located at the origin, but with the target point being as much as 0.2 inches from the origin (note, e.g., $y_A = 0.17$ in. in Table II), assuming γ_x and γ_y are zero could lead to cross section errors of a few parts in 10^4.

VIII. Target Angle Calibration

The target turntable is driven by a ring-and-pinion gear arrangement having an 8 to 1 reduction ratio. A high-quality ten-turn potentiometer connected to the driving shaft constitutes two arms of the bridge circuit shown in figure 24. The other two arms of the bridge are formed by a 40 turn potentiometer in the target controller chassis in the counting room. The position of the movable contact of the 10 turn pot, and therefore the angle of the target turntable, is compared with the position of the 40 turn pot by a sensitive null circuit. A reading of the turn counter connected to the latter potentiometer thus determines the target angle. We expect the turn counter to have a sensitivity of about $360°/(8 \times 4) = 11.25$ degrees/turn, so that the turn counter least count, 2×10^{-3} turns, corresponds to about 0.0225 degrees.

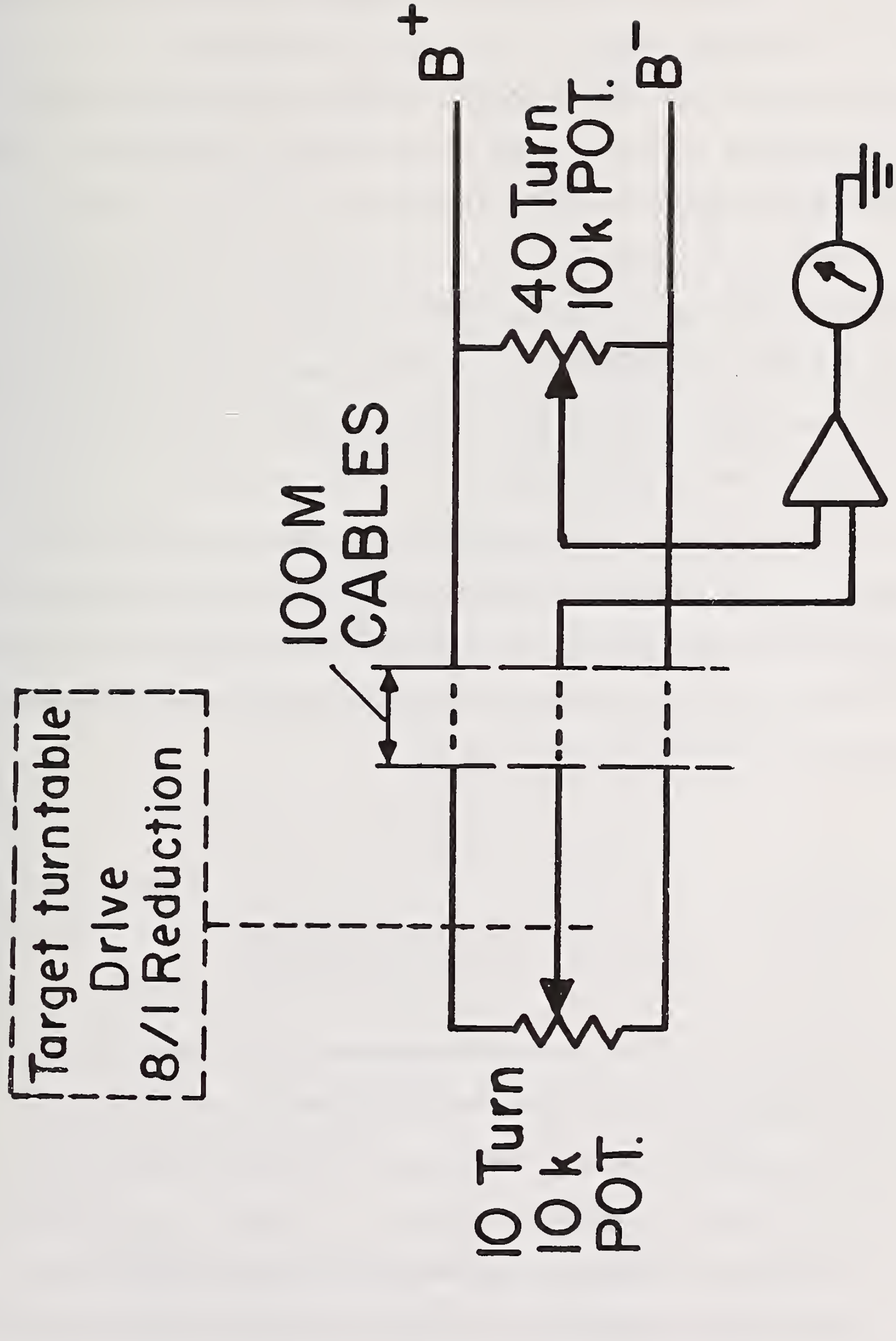

Figure 24. Target angle measuring circuit.

For scattering angles from 40 to 145 degrees, we normally perform experiments with the target bisecting the scattering angle, i.e., with $\theta_T \simeq \theta_o/2$. Our target angle calibration consists of finding the turn counter reading corresponding to each bisecting target angle for these seven values of θ_o. For each θ_o there are two values of θ_T, the second being obtained from the first by rotating the target turntable through 180° (and reversing the direction of the mirror in the target holder). The calibration is performed by optical sighting, using a setup similar to the one described in section VII for determining the angles γ_x and γ_y. The theodolite is set up on the baseline, pointing at the axis of rotation. The mirror mounted in a target holder is rotated, with the target turntable, until the theodolite cross hairs are aligned with the center of the horizontal aperture slits, with these slits closed to their limit position. For each θ_T, four independent measurements are made, two with the mirror aligned "up," and two with the mirror aligned "down;" the difference between up and down being a rotation of 180° about the normal to the mirror. Averaging up and down readings corrects for any angular error in locating the mirror in the target plane, but not for a translational misalignment. In addition to the values of θ_T corresponding to the bisector angles described above, calibrations of the turn counter by autocollimation were obtained at $\theta_T \simeq 0°$ and 180°--actually at $\theta_T = -0.005$ degrees because the theodolite was not precisely on the baseline for this calibration. All other calibrations are therefore at angles given by

$$\theta_T = (\theta_F - .005)/2$$

or

$$\theta_T = (\theta_F - .005)/2 + 180 \text{ degrees} ,$$

since the calibrations were performed with the spectrometer set at the fiducial angles.

A systematic difference between up and down mirror orientation of 1.2 ± 0.1 turn counter dial divisions was observed. A dial division is 10^{-2} turns, so the systematic difference corresponds to an angular misalignment of about 0.07 degrees. This misalignment does not affect the calibration because of the averaging of up and down readings.

Table V gives the target angle calibration in the form of the turn counter readings corresponding to each measured value of θ_T. Based on the reproducibility of individual measurements, the standard deviation of each dial setting should be about 0.5 divisions

(0.06 degrees). To check this error estimate, we make a least squares fit of the data in Table V to

$$T = a_1 + a_2\theta_T , \qquad (33)$$

where T is the turn counter reading in units of dial divisions. We find

$$a_1 = 823.5 \pm 0.6 \text{ divisions} ,$$

and (34)

$$a_2 = 8.752 \pm 0.004 \text{ divisions/degree} .$$

The standard deviation of each measurement for this fit is 1.3 divisions. If the enlarged deviations were caused by a translational misalignment, the effect would be

$$T(\theta_T + 180) - T(\theta_T) \propto \frac{a_2 \eta}{L_x} \sin \theta_T \qquad (35)$$

where η is the displacement of the mirror from the target plane. Since no correlation of this form is seen in the data, there is no significant translational error in mirror positioning. Further study of the deviations of the data from the straightline fit of eq (33) reveals a periodic variation which can be expressed by

$$T = a_1 + a_2\theta - 1.62 \cos 8(\theta + 5^\circ) , \qquad (36)$$

with a_1 and a_2 having the values given by eq (34). The fit of the data to eq (36) is much better than to eq (33), implying a standard deviation of 0.68 divisions or 0.08 degrees for each value of T in Table V, in reasonable agreement with our original estimate. The oscillatory term in eq (36) seems to have its origin in the 8 to 1 gear reduction of the turntable drive. An oscillation of the output angle of the vacuum feedthru in the rotation drive about the input angle with a 1.5° amplitude could produce the observed effect.

To use the target angle calibration the turn counter is set at one of the values given in Table V and the target pedestal rotated to obtain a null on the balancing circuit. This places the target at the corresponding angle to within 0.08 degrees standard deviation. If angles other than those listed in the table are required, or if the turn counter is accidentally set at a value not given in Table V, the target angle can be calculated from eq (34) and (36). In this case the error can be taken to be 0.08 degrees combined in quadrature with a small error due to the uncertainty in a_2.

IX. Summary

The experimental geometry is completely defined by the thirteen parameters θ_o, x_T, y_T, z_T, α_x, α_y, W, H, L_x, L_y, γ_x, γ_y, and R_s. In addition, θ_T is needed to calculate some of the above parameters and to obtain the effective target thickness W_o from the target foil thickness, t, from

$$W_o = t/\cos(\theta_T + \alpha_x)\cos\alpha_y \ . \tag{37}$$

The scattering angle, θ_o, is given by eq (26). The numerical constants $(\Delta\theta/\Delta\mathcal{D})$, $\mathcal{D}_F$, $(\Delta\theta/\Delta R)$, and R_F are summarized in Table VI, and the fiducial angles, θ_F, are listed in Table I. Determination of the dial gauge readings $\mathcal{D}$ and R are made for each experimental setup.

The target angle θ_T can be obtained from eq (36). It is best to use the fiducial target angles, θ_{TF}, and corresponding turn counter dial readings, T_F, listed in Table V. Performing a Taylor's series expansion on the small oscillatory term in eq (36), we find

$$\theta_T = \theta_{TF} + \frac{T - T_F}{a_2}\,[1 - a_3 \sin 8(\theta_{TF} + 5^\circ)] \ , \tag{38}$$

which is accurate to better than 10^{-3} degrees for $|T - T_F| < 2$ divisions. The numerical constants in eq (38) are given in Table VI.

The target coordinates x_T and z_T are obtained from measured quantities by eq (7). Expressions for x_B, η, x_p and z_p, which are needed to evaluate eq (7), are given by eq (5), (16), (17), and (18), respectively. The vertical coordinate of the target is given by

$$y_T = h - y_A \ , \tag{39}$$

after translating the coordinate origin to the height of the center of the Y slits. This translation is in accordance with the definition of the Y coordinate used in the computer program we use to calculate the solid angle and mean scattering angle. The constants

p_o, β, $\delta(180)$, $\delta(270)$, Δ, and S_v needed to evaluate eq (7) and (39) are listed in Table VI. The fiducial values $(A-C)_F$ and $(D-B)_F$ are given in Table I, and y_A is given in Table II. The parameters x_o and z_o are obtained for each experimental setup by the procedure described after eq (5) in section II. The step count $(N - N_o)_T$ is obtained from the online computer output of the beam scanners. Subscript T here specifies the horizontal scanner at the target location, for which $N_o = 100$. The remaining variables V, η', (A-C) and (D-B) must be measured for each experimental setup. Equation (6) cannot be used to determine h because of the unknown value of h_o, although this equation is useful for determining changes in h during data taking. We can determine h to sufficient accuracy ($\pm$ 1/32" or less) by visual observation of the beam spot on the standard bullseye, whose center is at $h = 0$.

The beam angles relative to the baseline are given by eq (8) and (9). Expressions for x_R, x_B, h, and x_p' are given by eq (4), (5), (6), and (19), respectively, and y_R is given by the analog of eq (4) for the vertical coordinates. The constants x_c, y_c, B_x, and B_y are given in Table II.

The origin-to-aperture distances are obtained from eq (27) and (29). The constants $\partial L_y/\partial R$, R_F, and ΔL are listed in Table VI, and the fiducial values $L_o(\theta_F)$ are given in Table I.

The aperture width and height, W and H, are simply the respective fringe counter readings, described in section II, minus the extrapolated readings at which the counting rates become zero. The standard deviations of the readings are 10^{-4} inches, and the uncertainty of the extrapolated-to-zero readings are statistical ones associated with the extrapolation.

The final parameter of the set is R_s which is listed in Table VI.

Constants listed in the tables have their corresponding uncertainty given, if that uncertainty affects the accuracy of the computed solid angle or mean scattering angle. All errors should be interpreted as one standard deviation. The propagation of the measurement errors into the uncertainty of a calculated cross section at a specified mean scattering angle is complicated because some of the measurement errors affect the final result in several ways. For example, an error in θ_o affects the calculated values of x_T, z_T, and α_x. The uncertainties given in Tables I, II, V, and VI are systematic in the sense that the actual (unknown) error affects all calculated cross sections, although not necessarily by the same amount. In addition, there are a number of sources of error which have random effects on individual cross section measurements. An intermediate class of uncertainties affect all cross sections measured at one nominal scattering angle systematically, but randomly for different scattering angles. For example, θ_T contains all three types of error (see eq 38): the uncertainty obtained by propagating the error in a_2 is systematic to all measurements; the uncertainty due to the calibration of fiducial values $\theta_{TF}(T_F)$ are systematic to all cross sections measured with a given θ_{TF} but independent for different values of θ_{TF}; and the error due to the settability of T($\pm$ 0.2 divisions) is random each time the target angle is set. Because of these complications, we cannot give overall error estimates here. We intend to study the effects of all sources of errors by numerical methods, using the computer programs which calculate the system geometry. In order to do this study, we need estimates of the random errors in the variables entering into the geometry parameters as well as the errors in the constants of Tables I, II, V, and VI. In the cases of x_o, z_o, the values of N occurring in eq (4), (5), and (6), and the aperture slit zero extrapolation, error estimates are obtained from the variance of the measurements. For the variables $\mathcal{D}$, $\mathcal{R}$, T, V, (A-C), (D-B), h, W, and H, our estimates of the associated random errors for a single measurement are summarized in Table VII.

The most important source of error is the irreproducible motion of the spectrometer on its carriage, discussed in section VII. The effect of this source of error on θ_o, L_x, and L_y is described by the measured correlations $\frac{\partial\theta_o}{\partial(D-B)}$ and $\frac{\partial L_o}{\partial(D-B)}$. The same source of error affects x_T through eq (7) and (17), z_T through eq (7) and (18), and α_x through eq (8) and (19). The target pedestal dial gauge effect influences the latter variables because we set the target pedestal at the position defined by the fiducial values of A-C and D-B, but these fiducial values as read on the gauges may be in error due to the irreproducible motion. The influence on x_T, z_T, and α_x can be obtained by differentiating the equations for these variables with respect to $(A-C)_F$ and $(D-B)_F$. It is important to note that the effect of this source of uncertainty on the several variables is completely correlated. In Table VIII, where we summarize these effects, we allow for this correlation by indicating the sign of each error term. The uncertainties in θ_o, L_x. L_y, x_T, z_T, and α_x for each setup of the spectrometer is obtained by multiplying the coefficients given in Table VIII by the standard deviation of a single setting of $(D-B)_F$ or $(A-C)_F$. All terms arising from $(D-B)_F$ are to be added algebraically, and then combined in quadrature with the terms arising from $(A-C)_F$. Thus, the total effect on the scattering angle of this source of error is given by

$$\Delta\theta = d\left\{\left[\frac{\partial\theta_o}{\partial(D-B)} + \frac{\partial\alpha_x}{\partial(D-B)_F}\right]^2 + \left[\frac{1}{L_x}\frac{\partial X_T}{\partial(A-C)_F} + \frac{\partial\alpha_x}{\partial(A-C)_F}\right]^2\right\}^{1/2} \qquad (40)$$

where $d = 2.2 \times 10^{-3}$ inches. At $\theta_o = 90°$, using $L_x = L_o(93°) + \Delta L$, $\Delta\theta = 6.7 \times 10^{-3}$ degrees. The effect of this error on the quoted value of a measured cross section is approximately 3 parts in 10^4. The effect on cross section entering through the solid angle calculation is much smaller because the error entering the solid angle through z_T is of opposite sign to that entering through L_x or L_y.

X. Acknowledgements

The precision mechanical devices needed to make the calibrations described in this report valid were designed and installed by the Mechanical Instrumentation Group of the NBS Nuclear Instrumentation Section. We wish to acknowledge the invaluable contribution of the members of this group: John Lantz, Dave Mohr, Joe Bradley, and Cliff Watkins. Without their dedicated efforts, this project could not have been completed successfully.

References

[1] "Experimental Apparatus Requirements for Accurate Electron Scattering Experiments," S. Penner and J. W. Lightbody, Jr., Internal Report No. 369, Nuclear Sciences Division, NBS, 1972 (unpublished).

[2] A more complete description of the entire system is given in "Experimental Techniques for Electron Scattering Investigations," Samuel Penner, NBS Technical Note 523 (1970), and references cited therein.

[3] J. S. Pruitt, Nucl. Instr. and Methods 92, 285 (1970).
J. S. Pruitt, Nucl. Instr. and Methods 100, 433 (1972).

[4] S. Penner and J. W. Lightbody, Jr., Proc. Int. Symposium on Magnet Technology, 154. Stanford Linear Accelerator Center, Stanford, California, CONF-650922 (1965).

[5] J. K. Whittaker, IEEE Trans. on Nucl. Sci. NS-19, 3, 444 (1972). A complete description of the performance of the detector system is being prepared.

[6] The device used is available commercially. Details of the operation are regarded as proprietary by the manufacturer.

Table I

Angle-Dependent Parameters Affecting the Scattering Angle and Solid Angle

Nominal Angle Degrees	Dial Guage Differences Fiducial Values, Inches		Fiducial Angle θ_F [a] Degrees	Fiducial Aperture Distance $L_o(\theta_F)$ [b] Inches
	$(D-B)_F$	$(A-C)_F$		
40	0.0300	0.0119	40.3491 ± 0.0041	21.0612 ± 0.0010
58	0.0337	0.0071	57.6031 ± 0.0040	21.0681 ± 0.0009
75	0.0334	0.0055	75.2602 ± 0.0040	21.0763 ± 0.0008
93	0.0321	0.0096	92.7753 ± 0.0039	21.0839 ± 0.0007
110	0.0309	0.0150	110.2659 ± 0.0038	21.0891 ± 0.0007
128	0.0305	0.0192	127.8827 ± 0.0037	21.0916 ± 0.0008
145	0.0311	0.0157	145.3855 ± 0.0037	21.0904 ± 0.0009
163	0.0297	0.0073	163.2745 ± 0.0036	21.0829 ± 0.0010
180	0.0259	-0.0032	180.0061 ± 0.0033	----

[a] The quoted uncertainties, which are standard deviations, are highly correlated for the various angles. The largest contribution to the total error is the error in the value of $\theta_F(180°)$, which is a common error for all other angles.

[b] The quoted uncertainties, which are standard deviations, contain a random measurement error of 0.0005 inches in each value. The remaining errors for L_o at various angles are correlated, with the largest contribution being 0.0004 inches due to the uncertainty in the measuring rod length (L_y in eq. [28]).

Table II

Quantities Measured Relative to Baseline

Quantity	Value	Standard Deviation	Units
$\theta_F(180)$ [a]	180.0061	± .0033	degrees
x_C	- 0.006	±0.008	inches
y_C	0.022	±0.009	inches
y_A	0.170	±0.012	inches
B_x	107.40	±0.05	inches
B_y	114.36	±0.05	inches

[a] Measured with R_F = 0.700 inches, $\mathcal{D}_F$ = 0.4902 inches, and (D-B) and (A-C) values given in Table I.

Table III

Sources of Error in Fiducial Angle Values [a]

Source	Magnitude (degrees)
$\theta_F(180)$, From Table II	3.3×10^{-3} [b]
$\theta_F(180)$, From Effects Listed Below	1.0 [b]
Theodolite Alignment	0.4
Theodolite Axis Offset	0.1
Uncertainties in $\delta(270)$ and $\delta(180)$	$\leq$1.8 [c]
Azimuthal Dial Gauge	0.0 [d]
Radial Dial Gauge Correction	$\leq$0.1
Target Pedestal Dial Gauge Correction	$\leq$0.3
Variance of Measurements	1.0
Total (combined in quadrature)	4.0×10^{-3}

[a] Does not apply to $\theta_F(180)$.

[b] These errors are common to all fiducial angles.

[c] From eq (21). Largest value of interest occurs at $\theta_F \simeq 40°$.

[d] No error since all data is taken at $\mathcal{D}=\mathcal{D}_F$.

Table IV

Errors in Origin to Aperture Slit Distance

Source	Standard Deviation (inches)
Effects entering through eq (28)	.0007 [a]
Uncertainty in $\partial L_y/\partial R$	$\leq$.0003 [b]
Target pedestal dial gauge effect	$\leq$.0008 [b]
Random measurement error	.0005
Total (combined in quadrature)	$\leq$.0012

[a] Error common to all values of $L_o(\theta_F)$.

[b] There is some correlation in the errors at various θ_F from these effects, but it can be neglected.

Table V

Results of Target Angle Calibration

Nominal Scattering Angle,[a] Degrees	θ_{TF} Degrees	T_F Dial Divisions	T_F for $\theta + 180.0^{\circ}$
163 [b]	- 8.363	751.7	2327.2
0	0.005[c]	822.8	2396.7
40	20.178	1001.7	2576.4
58	28.805	1075.4	2652.1
75	37.634	1152.3	2726.8
93	46.391	1227.8	2804.0
110	55.137	1307.0	2882.0
128	63.945	1384.2	2960.6
145	72.696	1460.0	3034.4

[a] The listed values of θ_{TF} orient the target for transmission scattering at these scattering angles, except as noted.

[b] Target is oriented for backscattering at a scattering angle of 163°. The listed target angle makes the path length in the target of incoming and scattered electrons equal.

[c] This target angle is used to calibrate the beam scanner as described in section II D.

Table VI Miscellaneous Constants

Quantity	Units	Value	Standard Deviation	Section Where Defined
$\left(\frac{\Delta\theta}{\Delta\mathcal{D}}\right)$	$\frac{\text{degrees}}{\text{inch}}$	-1.2566	0.0004	VI B
$\mathcal{D}_F$	inches	0.5[a]	--	VI B
$\left(\frac{\Delta\theta}{\Delta R}\right)$	$\frac{\text{degrees}}{\text{inch}}$	0.047	0.012	VI C
R_F	inches	0.7	--	VI C
a_2	$(\text{deg})^{-1}$	8.752	0.004	VIII
a_3	--	0.02585	--	IX
P_o	10^{-3}in	0	0.2	IV
β	10^{-4}rad	0.8	0.5	IV
$\delta(180)$	10^{-4}rad	0.9	0.7	IV
$\delta(270)$	10^{-4}rad	4.4	0.8	IV
Δ	10^{-3}in	2.83	0.03	IV
ρ	inch	1.25	0.03	II D
$\left(\frac{\partial L_y}{\partial R}\right)$	--	-1.0	0.006	VII
ΔL	inches	2.648	0.001	VII
R_s	inches	0.8750	0.0005	VIII
α_x	10^{-3}rad	5.0	1.0	VII
α_y	10^{-3}rad	-5.0	1.0	VII
S_v	--	1.156	.005	IV

[a] At $\theta_F = 180^\circ$, $\mathcal{D}_F = 0.4902$ inches.

Table VII

Estimated Errors (Inches) in Determination

Of Variable Parameters

Variable	Standard Deviation	Section Where Defined
$\mathcal{D}$	0.0002	VI B
$\mathcal{R}$	0.0005	VI C
T	0.68	VIII
V	0.25	IV
A-C	0.0003	--
D-B	0.0003	--
h	0.02	II D
W	0.0001 [a]	II B
H	0.0001 [a]	II B

[a] This error is in addition to, and independent of, the error in determining the reference opening of the slits. The latter error is obtained from the extrapolation to the zero-count-rate opening, discussed in section II B.

Table VIII

Errors Due to Target Pedestal Dial Gauge Effect

The use of the terms listed in obtaining the errors in the experiment is described in section IX.

Variable Affected	Function	Value
θ_o	$\frac{\partial \theta_o}{\partial (D-B)}$	$2.52 \pm 0.44 \frac{\text{deg.}}{\text{in}}$
L_x	$\frac{\partial L_o}{\partial (D-B)}$	$- 0.94 \pm 0.30$
L_y	$\frac{\partial L_o}{\partial (D-B)}$	0.94 ± 0.30
x_T	$\frac{\partial X_T}{\partial (A-C)_F} = \frac{S_v}{2}$	0.578 ± 0.003
z_T	$\frac{\partial Z_T}{\partial (D-B)_F} = - \frac{S_v}{2}$	-0.578 ± 0.003
α_x	$\frac{\partial \alpha_x}{\partial (D-B)_F} = \frac{S_v}{2B_x} \cos \theta_o$	$(5.38 \pm 0.02) \times 10^{-3} \cos\theta_o \text{in}^{-1}$
	$\frac{\partial \alpha_x}{\partial (A-C)_F} = - \frac{S_v}{2B_x} \sin \theta_o$	$-(5.38 \pm 0.02) \times 10^{-3} \sin\theta_o \text{in}^{-1}$

NBS-114A (REV. 7-73)

U.S. DEPT. OF COMM. BIBLIOGRAPHIC DATA SHEET	1. PUBLICATION OR REPORT NO. NBS TN-871	2. Gov't Accession No.	3. Recipient's Accession No.
4. TITLE AND SUBTITLE Geometrical Calibration of the NBS Electron Scattering Apparatus			5. Publication Date June 1975 6. Performing Organization Code
7. AUTHOR(S) S. Penner, S. P. Fivozinsky, J. W. Lightbody, Jr., L. S. Cardman, and W. P. Trower			8. Performing Organ. Report No.
9. PERFORMING ORGANIZATION NAME AND ADDRESS NATIONAL BUREAU OF STANDARDS DEPARTMENT OF COMMERCE WASHINGTON, D.C. 20234			10. Project/Task/Work Unit No. 11. Contract/Grant No.
12. Sponsoring Organization Name and Complete Address (Street, City, State, ZIP) Research Corporation of New York 405 Lexington Avenue New York, New York 10017 U. S. Energy Research and Development Administration Washington, D. C. 20545			13. Type of Report & Period Covered Final 14. Sponsoring Agency Code

15. SUPPLEMENTARY NOTES

16. ABSTRACT *(A 200-word or less factual summary of most significant information. If document includes a significant bibliography or literature survey, mention it here.)*

A comprehensive calibration of the geometry of the NBS electron scattering apparatus is described. A complete set of measured parameters is tabulated in this report. Combining these parameters with observed values of certain variables as described herein permits the accurate determination of the solid angle, scattering angle, and target angle for each cross section measurement made with the apparatus. The uncertainty in a cross section measurement due to the imprecision of the geometry calibrations is less than one part in 10^3.

17. KEY WORDS *(six to twelve entries; alphabetical order; capitalize only the first letter of the first key word unless a proper name; separated by semicolons)*

Absolute cross section; beam profile; electron scattering; scattering angle; solid angle; spectrometer

18. AVAILABILITY	19. SECURITY CLASS (THIS REPORT)	21. NO. OF PAGES
[XX] Unlimited [ ] For Official Distribution. Do Not Release to NTIS	UNCLASSIFIED	79
[XX] Order From Sup. of Doc., U.S. Government Printing Office Washington, D.C. 20402, SD Cat. No. C13.46:871 [ ] Order From National Technical Information Service (NTIS) Springfield, Virginia 22151	20. SECURITY CLASS (THIS PAGE) UNCLASSIFIED	22. Price $1.40

USCOMM-DC 29042-P74

NBS TECHNICAL PUBLICATIONS

PERIODICALS

JOURNAL OF RESEARCH reports National Bureau of Standards research and development in physics, mathematics, and chemistry. It is published in two sections, available separately:

- **Physics and Chemistry (Section A)**

Papers of interest primarily to scientists working in these fields. This section covers a broad range of physical and chemical research, with major emphasis on standards of physical measurement, fundamental constants, and properties of matter. Issued six times a year. Annual subscription: Domestic, $17.00; Foreign, $21.25.

- **Mathematical Sciences (Section B)**

Studies and compilations designed mainly for the mathematician and theoretical physicist. Topics in mathematical statistics, theory of experiment design, numerical analysis, theoretical physics and chemistry, logical design and programming of computers and computer systems. Short numerical tables. Issued quarterly. Annual subscription: Domestic, $9.00; Foreign, $11.25.

DIMENSIONS/NBS (formerly Technical News Bulletin)—This monthly magazine is published to inform scientists, engineers, businessmen, industry, teachers, students, and consumers of the latest advances in science and technology, with primary emphasis on the work at NBS. The magazine highlights and reviews such issues as energy research, fire protection, building technology, metric conversion, pollution abatement, health and safety, and consumer product performance. In addition, it reports the results of Bureau programs in measurement standards and techniques, properties of matter and materials, engineering standards and services, instrumentation, and automatic data processing.

Annual subscription: Domestic, $9.45; Foreign, $11.85.

NONPERIODICALS

Monographs—Major contributions to the technical literature on various subjects related to the Bureau's scientific and technical activities.

Handbooks—Recommended codes of engineering and industrial practice (including safety codes) developed in cooperation with interested industries, professional organizations, and regulatory bodies.

Special Publications—Include proceedings of conferences sponsored by NBS, NBS annual reports, and other special publications appropriate to this grouping such as wall charts, pocket cards, and bibliographies.

Applied Mathematics Series—Mathematical tables, manuals, and studies of special interest to physicists, engineers, chemists, biologists, mathematicians, computer programmers, and others engaged in scientific and technical work.

National Standard Reference Data Series—Provides quantitative data on the physical and chemical properties of materials, compiled from the world's literature and critically evaluated. Developed under a world-wide program coordinated by NBS. Program under authority of National Standard Data Act (Public Law 90-396).

NOTE: At present the principal publication outlet for these data is the Journal of Physical and Chemical Reference Data (JPCRD) published quarterly for NBS by the American Chemical Society (ACS) and the American Institute of Physics (AIP). Subscriptions, reprints, and supplements available from ACS, 1155 Sixteenth St. N. W., Wash. D. C. 20056.

Building Science Series—Disseminates technical information developed at the Bureau on building materials, components, systems, and whole structures. The series presents research results, test methods, and performance criteria related to the structural and environmental functions and the durability and safety characteristics of building elements and systems.

Technical Notes—Studies or reports which are complete in themselves but restrictive in their treatment of a subject. Analogous to monographs but not so comprehensive in scope or definitive in treatment of the subject area. Often serve as a vehicle for final reports of work performed at NBS under the sponsorship of other government agencies.

Voluntary Product Standards—Developed under procedures published by the Department of Commerce in Part 10, Title 15, of the Code of Federal Regulations. The purpose of the standards is to establish nationally recognized requirements for products, and to provide all concerned interests with a basis for common understanding of the characteristics of the products. NBS administers this program as a supplement to the activities of the private sector standardizing organizations.

Federal Information Processing Standards Publications (FIPS PUBS)—Publications in this series collectively constitute the Federal Information Processing Standards Register. Register serves as the official source of information in the Federal Government regarding standards issued by NBS pursuant to the Federal Property and Administrative Services Act of 1949 as amended, Public Law 89-306 (79 Stat. 1127), and as implemented by Executive Order 11717 (38 FR 12315, dated May 11, 1973) and Part 6 of Title 15 CFR (Code of Federal Regulations).

Consumer Information Series—Practical information, based on NBS research and experience, covering areas of interest to the consumer. Easily understandable language and illustrations provide useful background knowledge for shopping in today's technological marketplace.

NBS Interagency Reports (NBSIR)—A special series of interim or final reports on work performed by NBS for outside sponsors (both government and non-government). In general, initial distribution is handled by the sponsor; public distribution is by the National Technical Information Service (Springfield, Va. 22161) in paper copy or microfiche form.

Order NBS publications (except NBSIR's and Bibliographic Subscription Services) from: Superintendent of Documents, Government Printing Office, Washington, D.C. 20402.

BIBLIOGRAPHIC SUBSCRIPTION SERVICES

The following current-awareness and literature-survey bibliographies are issued periodically by the Bureau:

Cryogenic Data Center Current Awareness Service

A literature survey issued biweekly. Annual subscription: Domestic, $20.00; foreign, $25.00.

Liquefied Natural Gas. A literature survey issued quarterly. Annual subscription: $20.00.

Superconducting Devices and Materials. A literature survey issued quarterly. Annual subscription: $20.00. Send subscription orders and remittances for the preceding bibliographic services to National Technical Information Service, Springfield, Va. 22161.

Electromagnetic Metrology Current Awareness Service

Issued monthly. Annual subscription: $100.00 (Special rates for multi-subscriptions). Send subscription order and remittance to Electromagnetics Division, National Bureau of Standards, Boulder, Colo. 80302.

U.S. DEPARTMENT OF COMMERCE
National Bureau of Standards
Washington, D.C. 20234

OFFICIAL BUSINESS

Penalty for Private Use, $300

POSTAGE AND FEES PAID
U.S. DEPARTMENT OF COMMERCE
COM-215

SPECIAL FOURTH-CLASS RATE
BOOK